

Mini Review

Open Access



# Advances in lithium-ion battery materials for ceramic fuel cells

Xiaomi Zhou<sup>1,#</sup>, Jingjing Yang<sup>2,#</sup>, Ruoming Wang<sup>2</sup>, Wei Zhang<sup>3,\*</sup>, Sining Yun<sup>2,\*</sup>, Baoyuan Wang<sup>1,\*</sup>

<sup>1</sup>School of Microelectronics, Hubei University, Wuhan 430062, Hubei, China.

<sup>2</sup>Functional Materials Laboratory, School of Materials Science and Engineering, Xi'an University of Architecture and Technology, Xi'an 710055, Shaanxi, China.

<sup>3</sup>Department of Materials Science and Engineering, Michigan Technological University, Houghton, MI 49931, USA.

#Authors contributed equally.

\***Correspondence to:** Wei Zhang, Department of Materials Science and Engineering, Michigan Technological University, 1400 Townsend Dr., Houghton, MI 49931, USA. E-mail: wzhang9@mtu.edu; Prof./Dr. Sining Yun, Functional Materials Laboratory, School of Materials Science and Engineering, Xi'an University of Architecture and Technology, No. 13, Yanta Road, Yanta District, Xi'an 710055, Shaanxi, China. E-mail: yunsining@xauat.edu.cn; Prof./Dr. Baoyuan Wang, School of Microelectronics, Hubei University, No. 368, Friendship Avenue, Wuchang District, Wuhan 430062, Hubei, China. E-mail: baoyuanw@163.com

**How to cite this article:** Zhou X, Yang J, Wang R, Zhang W, Yun S, Wang B. Advances in lithium-ion battery materials for ceramic fuel cells. *Energy Mater* 2022;2:200041. <https://dx.doi.org/10.20517/energymater.2022.76>

**Received:** 10 Nov 2022 **Accepted:** 1 Dec 2022 **Published:** 13 Dec 2022

**Academic Editor:** Yuping Wu **Copy Editor:** Fangling Lan **Production Editor:** Fangling Lan

## Abstract

Lithium-ion batteries (LIBs) and ceramic fuel cells (CFCs) are important for energy storage and conversion technologies and their materials are central to developing advanced applications. Although there are many crosslinking research activities, e.g., through materials and some common scientific fundamentals employed for both LIB and CFCs, crosslinking scientific aspects to achieve a comprehensive understanding are missing. There is a lack of such a review to promote and guide further research and development in the crosslinking of LIBs and CFCs. Herein, we review the existing application of LIB materials in CFCs to discover the scientific advances of lithium-ion and proton transport cooperation and identify the new directions of Li-CFCs in the future. This review is the first to propose CFC advances, especially at low temperatures (300-600 °C) by applying LIB materials to practical devices and highlight the material properties and new device functions with enhanced performance, as well as the scientific mechanisms and principles. Furthermore, we seek to deepen the scientific understanding of materials science, ion transport mechanisms and semiconductor electrochemistry to benefit both the battery and fuel cell fields.



© The Author(s) 2022. **Open Access** This article is licensed under a Creative Commons Attribution 4.0 International License (<https://creativecommons.org/licenses/by/4.0/>), which permits unrestricted use, sharing, adaptation, distribution and reproduction in any medium or format, for any purpose, even commercially, as long as you give appropriate credit to the original author(s) and the source, provide a link to the Creative Commons license, and indicate if changes were made.



**Keywords:** Lithium-ion batteries, ceramic fuel cells, built-in electric field, semiconducting materials

## INTRODUCTION

Fossil energy must be replaced by clean and sustainable energy. Due to the large storage capacity of water, hydrogen energy obtained by the electrolysis of water is likely to play an important role in future energy sources, especially from seawater<sup>[1]</sup>. Ceramic fuel cells (CFCs), including solid oxide fuel cells (SOFCs), proton ceramic fuel cells (PCFCs), ceria-carbonate composite fuel cells and semiconductor membrane fuel cells<sup>[2]</sup>, have attracted significant attention due to their highly efficient utilization of H<sub>2</sub> fuel, which can convert chemical to electrical energy directly with high efficiency<sup>[3]</sup>. As shown in Figure 1A, a CFC can be divided into three parts, namely, an anode, cathode and electrolyte. Generally, the oxygen reduction reaction (ORR) at the cathode and the hydrogen oxidation reaction (HOR) at the anode require efficient and stable electrocatalytic materials to facilitate the electrode reactions. The electrolyte not only avoids the direct thermal combustion between hydrogen and oxygen but also transports the ions (O<sup>2-</sup> and H<sup>+</sup>) while blocking redundant electron leakage from the HOR. Obviously, the excess electricity generated by fuel combustion can be stored for continuous use by energy storage devices.

Lithium-ion batteries (LIBs) have occupied an indispensable position in energy storage devices. Due to their advantages of portability, environmental friendliness, small size and lightweight, LIBs are widely used in electric vehicles and mobile electronic devices<sup>[4]</sup>. As shown in Figure 1B, the physical structure of a LIB is similar to that of a CFC, with a cathode, anode and electrolyte; however, the three components play different roles in LIBs. Lithium ions are released from the cathode and intercalated in the anode during charging and this process is reversed when discharging. The electrolyte provides a place for lithium ions to shuttle between the cathode and anode<sup>[5]</sup>. As an efficient energy conversion device, however, the practical application of CFCs has been restricted by their severe operating requirements (e.g., high operating temperature) compared with the room-temperature operation of LIBs.

As the state-of-the-art commercial electrolyte material in CFCs, 8 mol.% yttrium stabilized zirconia (YSZ) exhibits an appreciable conductivity (0.1 S/cm) but only at a high temperature of ~1000 °C<sup>[6]</sup>. High temperatures result in significant challenges to devices, such as reduced stability, limitations regarding application sites and high manufacturing costs, which restrict commercial development. Based on the current state of development, exploring low-temperature (300-600 °C) CFCs is more meaningful and challenging<sup>[7]</sup>. Sebastian *et al.* reported that reversible ion exchange occurred when replacing Li<sup>+</sup> with H<sup>+</sup> in a LIB material, which implies that a LIB material can turn into a proton conductor<sup>[8]</sup>. All-solid-state LIBs with high lithium-ion conductivity will drive the development of low-temperature CFCs based on proton conductors. Wei *et al.* found that Sr-doped Li<sub>1.3</sub>Sr<sub>0.1</sub>Zn(GeO<sub>4</sub>)<sub>4</sub> exhibited high conductivity for lithium ions and protons under fuel cell operating conditions<sup>[9]</sup>. The pathway for H<sup>+</sup> is from one site to another in the three-dimensional Li<sup>+</sup> transport network. The Li<sup>+</sup> and H<sup>+</sup> interacting transport mechanism has been deeply studied, including exchange, coupling and so on, which provides a strong basis for the application of LIB materials in fuel cells and drives the development of fuel cell devices to low temperatures.

In addition to electrolytes, LIB materials have also been successfully used as fuel cell electrodes. A typical example is Ni<sub>0.8</sub>Co<sub>0.15</sub>Al<sub>0.05</sub>Li-oxide (NCAL), which possesses excellent electrocatalytic properties as an electrode material for CFCs and shows significant potential for replacing traditional noble metal- and multi-element-doped oxide-based electrodes<sup>[10]</sup>. Despite some differences in the ionic species in the electrolyte, there is a high similarity between the operating principles of LIBs and CFCs, namely, both of them are electrochemical devices based on redox reactions at the anode and cathode to convert chemical energy to

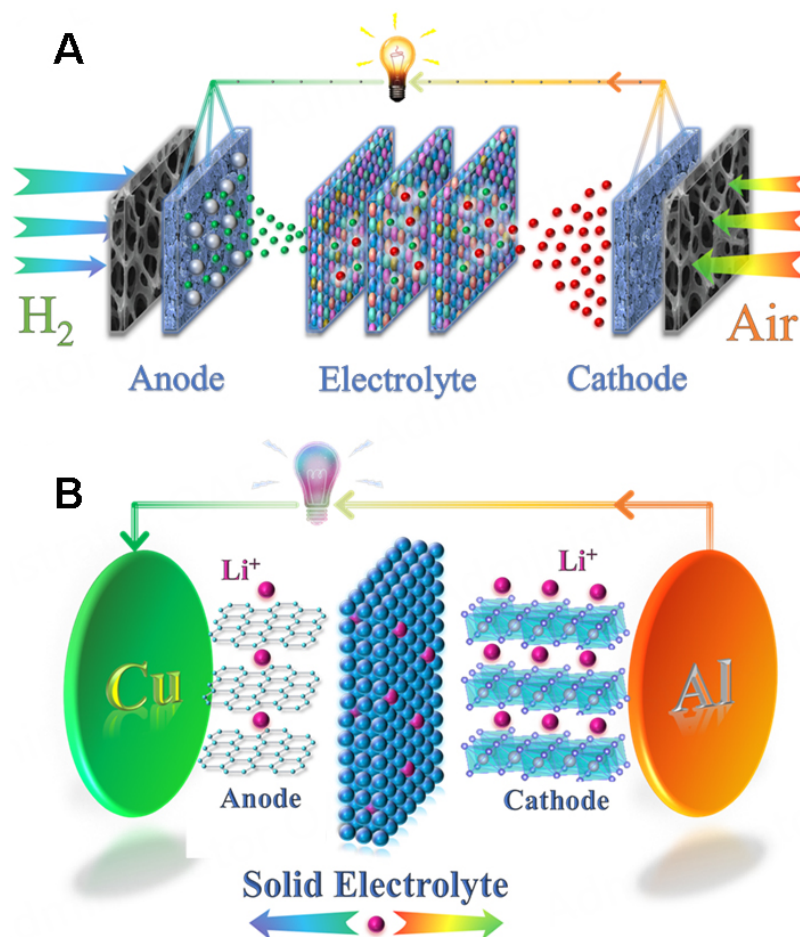


**Figure 1.** Schematic illustrations of a (A) CFC and (B) LIB. CFC: Ceramic fuel cell; LIB: lithium-ion battery.

electricity. It is noteworthy that in recent research and developments for both LIBs and CFCs, semiconducting properties<sup>[11]</sup>, electronic states<sup>[12]</sup>, band structure and built-in electric field (BIEF) effects<sup>[13]</sup> have been introduced into electrochemical devices to improve and enhance the ion transfer in electrode dynamics for enhanced high rate cycling and device durability<sup>[14]</sup>. These factors also help to improve the energy storage capacity and performance of devices<sup>[15]</sup>. In addition, there is an important common principle for the space-charge layer (SCL) effect on interfacial ion transport in all-solid-state batteries and CFCs<sup>[16]</sup>. Thus, significant efforts have been stimulated to investigate the crosslinking transport mechanism between lithium-ion and proton/oxygen ion transport in novel CFCs. LIB materials also exhibited excellent catalytic properties for hydrogen oxidation and oxygen reduction in CFCs<sup>[17]</sup>, which can effectively reduce the operating temperature of CFCs by using low-temperature electrolyte materials for practical applications<sup>[18]</sup>. LIB materials used in CFCs provide an attractive research direction for the future development of CFCs<sup>[19,20]</sup>.

### CROSSLINKING METHODOLOGY OF LIBS AND CFCs

Based on the state-of-the-art applications of LIB materials in CFCs and their crosslinking methodologies, as well as common material properties and scientific principles, we can make the following perspectives to facilitate further research and development to crosslink these two important fields.

### Semiconducting properties of materials

The semiconducting properties of materials are the basic scientific principles for supporting the high-performance output of CFCs. Related applications have also attracted significant attention in the fields of LIBs, Na-ion batteries and Zn-ion batteries. From the work of Ensling *et al.*, the Li<sup>+</sup> deintercalation of Li<sub>x</sub>CO<sub>2</sub> thin-film cathode materials led to the evolution of the electronic structure, as shown in Figure 2A<sup>[11]</sup>. From the Li<sup>+</sup> removal, Co<sup>3+</sup> was oxidized to Co<sup>4+</sup> and the electronic state at the oxygen site was stable. Furthermore, the Fermi level was lowered and the electronic density of states deviated. The top of the O<sub>2p</sub> band overlapped with the Co<sub>3d</sub> state, with the hole transferred to the O<sub>2p</sub> states. The density of states (DOS) showed that the deep Li deintercalation had an important impact on the band structure of Li<sub>1-x</sub>CoO<sub>2</sub><sup>[11]</sup>. For the CFC cathode material Sb-doped Ba<sub>0.5</sub>Sr<sub>0.5</sub>FeO<sub>3-δ</sub> perovskite oxide, Sb doping could enhance the electrical conductivity and ORR activity. The DOS of the p and d band centers shifts near the Fermi level with Sb doping, as shown in Figure 2B, which can increase the efficiency of electron transfer to the adsorbed oxygen species O<sub>2</sub>. The higher DOS induced by Sb provided faster kinetics of charge transfer<sup>[21]</sup>. Exploring the semiconducting properties of materials inspires us to define electrical energy devices from another perspective. The introduction of external ions into the lattice changes the DOS of the substrate material, resulting in variations in the semiconducting properties of the materials. It is necessary to consider the semiconducting properties of the materials as they can directly affect the output properties of the device.

### Electrochemical principles of semiconductors in LIBs and CFCs

In LIBs and CFCs, charged ions pass from the cathode, anode, dissociate through the electrolyte and bring energy conversion according to electrochemical methods. The semiconducting properties and energy band theory can improve electrochemical kinetics and increase the transport rate. Crosslinking methods promote the scientific understanding of electrochemical devices. Generally, the energy band is closely associated with the charge transfer. The opposite charges were left at the interface between the electrode and electrolyte, leading to the generation of a Helmholtz double layer on the electrolyte side<sup>[22]</sup>. The free e<sup>-</sup> in the conduction band and h<sup>+</sup> from the valence band of the electrode exchange their charges in the diffusion processes with the electrolyte, resulting in charge accumulation at the surface<sup>[23]</sup> and band bending formed at the interface (as shown in Figure 3A) with the Fermi level, thereby achieving an equilibrium position. In CFCs, n- and p-type semiconductors can maintain the BIEF to block electron penetration and enhance the ion transport, with a one-interface device being used instead of two interfaces (anode/electrolyte and cathode/electrolyte), as shown in Figure 3B. In a LIB system, the DOS of the LiCoO<sub>2</sub> positive electrode are related to the Fermi level of the Co<sup>4+/3+</sup> redox couple, as demonstrated in Figure 3C, pertaining to the highest occupied molecular orbital (HOMO) and the lowest unoccupied molecular orbital (LUMO) of the liquid electrolyte. To keep a LIB working properly, the chemical potential of the electrode must be controlled in the energy gap between the HOMO and LUMO. From the electrolyte interface of the double-layer LiCoO<sub>2</sub>/diethyl carbonate (DEC) (alkyl carbonate solvent) electrolyte reported by Becker *et al.*, the Li ion energy level bent in the opposite direction to the energy level of the electrons<sup>[24]</sup>. The diffusion of Li ions through the charge layer at interfaces caused the band bending, as illustrated by Figure 3D, and the changing of the charge carrier concentration had a non-negligible impact on the charge transfer rate.

The double-layer electrolyte model for CFCs is also suitable. In a report by Wang *et al.*, CeO<sub>2</sub> on the air side showed hole (p-type) conduction and reduced CeO<sub>2</sub> (R-CeO<sub>2</sub>) on the H<sub>2</sub> side turned to electron (n-type) conduction<sup>[25]</sup>. The band energy alignment between p-type CeO<sub>2</sub> and n-type R-CeO<sub>2</sub> facilitated the charge separation and blocked the excess electrons, as shown in Figure 3E. The oxygen vacancy as a two-electron donor center converted Ce<sup>4+</sup> to Ce<sup>3+</sup>. Based on the generation process of Ce<sup>3+</sup> and oxygen vacancies at the interface, a double-layer cell structure was formed due to the p-n junction, while the surface and grain boundaries can promote ion transport. From the work of Xing *et al.*, the N-N 3C-SiC/ZnO heterostructure electrolyte in a CFC exhibited an improved ionic conductivity of 0.12 S/cm through the energy band

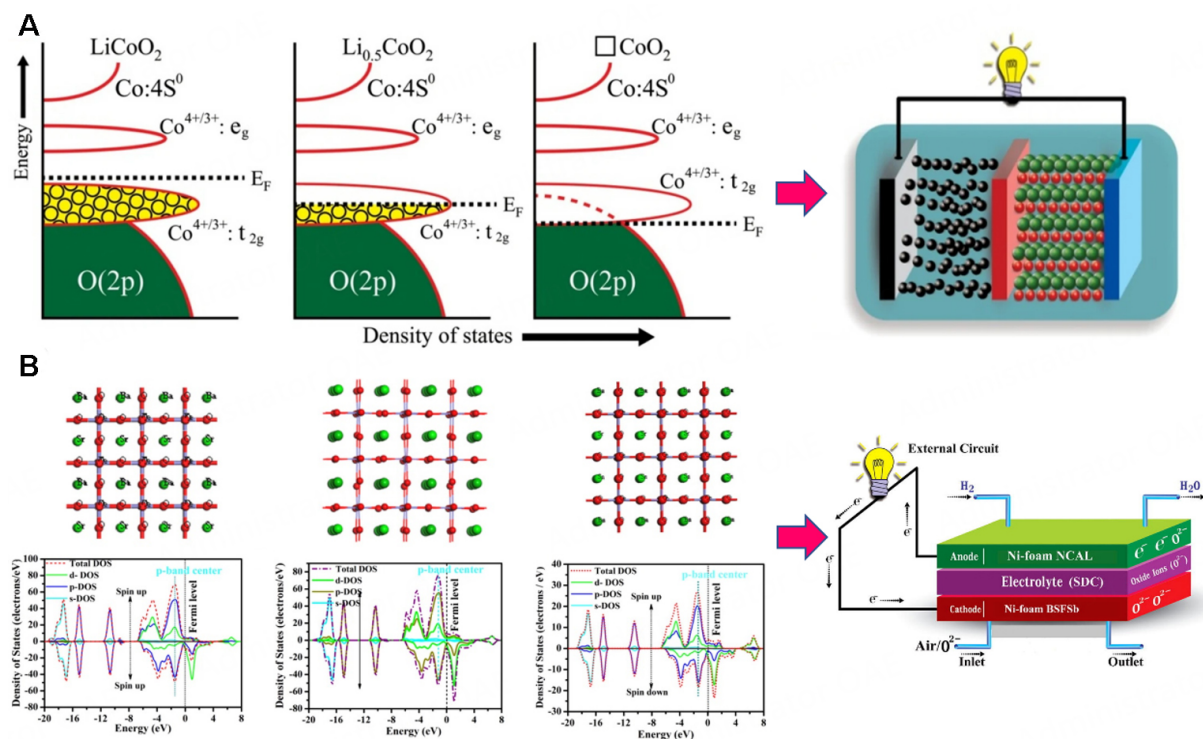


**Figure 2.** (A) Electronic band structure of LiCoO<sub>2</sub> cathode in a LIB (Li = 1, left), Li<sub>0.5</sub>CoO<sub>2</sub> (Li = 0.5, middle) and CoO<sub>2</sub> (Li = 0, right). Copyright from Ref.<sup>[11]</sup>. (B) Optimized structure and electron PDOS calculated by density functional theory for Ba<sub>0.5</sub>Sr<sub>0.5</sub>Fe<sub>1-x</sub>Sb<sub>x</sub>O<sub>3.8</sub> (x = 0, left; x = 0.05, middle; x = 0.1, right) Copyright from Ref.<sup>[21]</sup>.

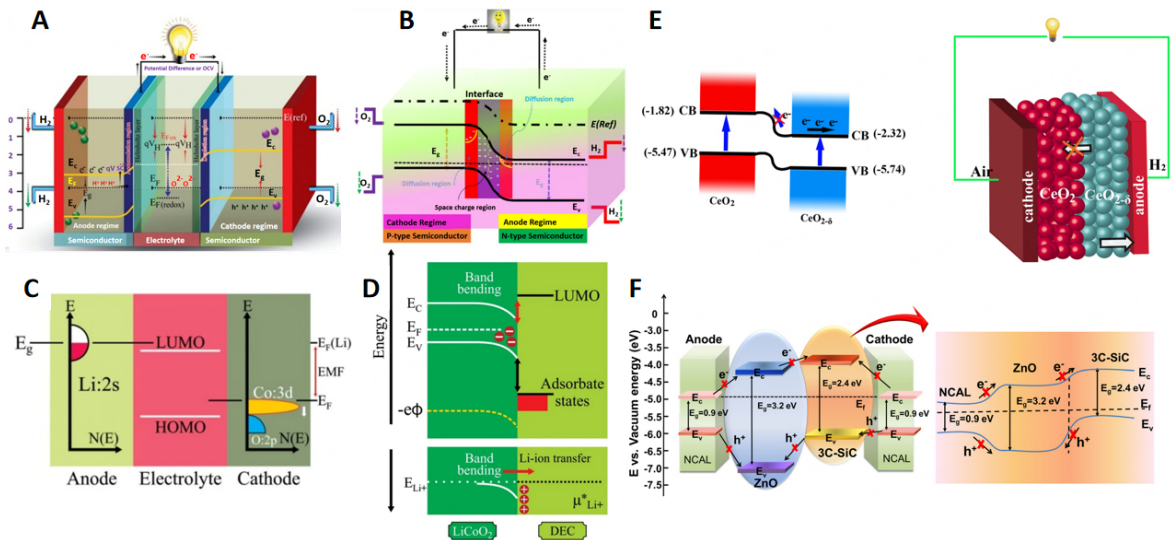


**Figure 3.** An overview of LIB and CFC band structures from semiconductor electrochemical aspects. (A) Schematic of working principle and energy diagram at LIB/CFC electrode (semiconductor) interface with the electrolyte, in which the Fermi levels are in equilibrium positions. Copyright from Ref.<sup>[22]</sup>. (B) Schematic of working principle and energy diagram for a CFC without an electrolyte, Copyright from Ref.<sup>[22]</sup>. (C) Relative energy positions of LiCoO<sub>2</sub> cathode with respect to HOMO and LUMO of liquid electrolyte in a LIB. Copyright from Ref.<sup>[11]</sup>. (D) Energy level diagram of LiCoO<sub>2</sub>/DEC interface established from low-temperature adsorption of DEC (alkyl carbonate solvent) electrolyte. Copyright from Ref.<sup>[24]</sup>. (E) Band bending and alignment occurring in CeO<sub>2</sub> electrolyte CFC, resulting in a double-layer device due to P/N junction formed under H<sub>2</sub>/air fuel cell conditions. Copyright from Ref.<sup>[25]</sup>. (F) Band bending and alignment situation and device working principle for semiconductor cubic silicon carbide (3C-SiC)/ZnO electrolyte in a CFC. Copyright from Ref.<sup>[26]</sup>.

alignment methodology in [Figure 3F](#)<sup>[26]</sup>. The enrichment of charged ions at the interface has a positive effect on ion transport. Band bending due to ion aggregation is a guarantee for continuous movement. This methodology plays an important role in electrochemical devices.

### Impact of BIEF on electrochemical performance of LIBs and CFCs

The common characteristic of the semiconductor and energy band theories in LIBs and CFCs is that the band alignment induces a BIEF, which has an enhancement effect on the electrochemical performance, especially regarding the promotion of ion transport<sup>[27]</sup>. The BIEF can also improve the cycle life and fast discharge-charge cycling and enlarge the capacity in LIBs. A BIEF at the semiconductor particle level has been reported by Xia *et al.* for a TiO<sub>2</sub>-based electrode, as shown in [Figure 4A](#), which accelerated electrode Li intercalation at high charge-discharge rates and promoted the Li-ion diffusion process<sup>[13]</sup>. Another Li-ion migration mechanism is also important, namely, the SCL, which is widely discussed for solid-state lithium batteries. The concept is that a SCL is formed by continuous charge distributed in a space but not a point of charge. The electron cloud of charge and carriers fully diffuses in the solid area to form the space charge region, similar to the p-n junction in semiconductors. First-principles calculations [[Figure 4B](#)] showed that Li-ion migration across the interface between the cathode and electrolyte depended on the higher lithium chemical potential site and potential energy surfaces, which can cause dynamic Li<sup>+</sup> depletion with interfacial electron transfer<sup>[28]</sup>. In-situ differential phase contrast scanning transmission electron microscopy and finite element simulations were used to identify a BIEF, indicating a reduced SCL and boosted Li<sup>+</sup> transmission, in all-solid-state LIBs<sup>[29]</sup>. The migration mechanism of Li ions is favorable for observing the movement process of protons, electrons and oxygen ions, and finding the key factors for the working process of LIB materials in fuel cells.

Similarly, the construction of a BIEF has also been demonstrated to be very effective in developing high-performance Na-ion batteries, as reported by Ni *et al.*<sup>[30]</sup>. [Figure 4C](#) illustrates a BIEF spontaneously formed at the heterogeneous interface of n-Fe<sub>2</sub>O<sub>3</sub> and p-FeS<sub>2</sub>. During discharge (sodiation), the Na<sup>+</sup> was driven by the BIEF from n-type Fe<sub>2</sub>O<sub>3</sub> to p-type FeS<sub>2</sub>, resulting in an enhancement in transport kinetics. For recharging, the opposite process of Na<sup>+</sup> desodiation made a new BIEF directing from FeS<sub>2</sub> to Fe<sub>2</sub>O<sub>3</sub>. Consequently, the BIEF consistently enhances the Na<sup>+</sup> diffusion kinetics in the S-Fe<sub>2</sub>O<sub>3</sub> system. Our current understanding of the transport mechanisms from BIEFs provides a new direction for CFC research. The BIEF mechanism has been widely applied to develop advanced CFCs. A Sm<sub>2</sub>O<sub>3</sub>/Ni-Sm<sub>2</sub>O<sub>3</sub> core shell homostructure was proposed to accelerate proton transport, as shown in [Figure 4D](#). With Ni surface modification, the increased oxygen vacancies provided transport channels for protons and the local electric field of the Sm<sub>2</sub>O<sub>3</sub>/Ni-Sm<sub>2</sub>O<sub>3</sub> homostructure confined the proton migration only in the highly conductive surface layer<sup>[31]</sup>. Xing *et al.* reported that proton conduction was enhanced because of the BIEF in a CeO<sub>2</sub>/CeO<sub>2.5</sub> core-shell structure, as illustrated by [Figure 4E](#)<sup>[32]</sup>. The electronic state changed due to the concentration of oxygen vacancies increasing in CeO<sub>2.5</sub>. The charge separation at the surface of CeO<sub>2.5</sub>/CeO<sub>2</sub> limited proton transmission through the near-surface layer of the particle. Although BIEFs are generally instructive for electrochemical devices, the relevant applications of BIEFs in LIBs have implications for CFCs.

### Promoting performance by LIB and CFC crosslinking

Although the working mechanisms in electrochemical devices are different, the promotion of ion diffusion by different methodologies has a strong correlation. Li<sup>+</sup> conduction highly relies on lithium vacancies in solid oxides and a well-designed Li<sup>+</sup> concentration and an optimized occupancy rate can enhance the ionic conductivity<sup>[33]</sup>. Thus, clarifying the transport mechanism of Li<sup>+</sup> is necessary to improve the conductivity. For LiFePO<sub>4</sub> with an olivine-type structure<sup>[34]</sup>, the calculation results in [Figure 5A](#) show that Li ions migrating along the [010] direction have a lower activation energy (0.27 eV) and a continuous curved

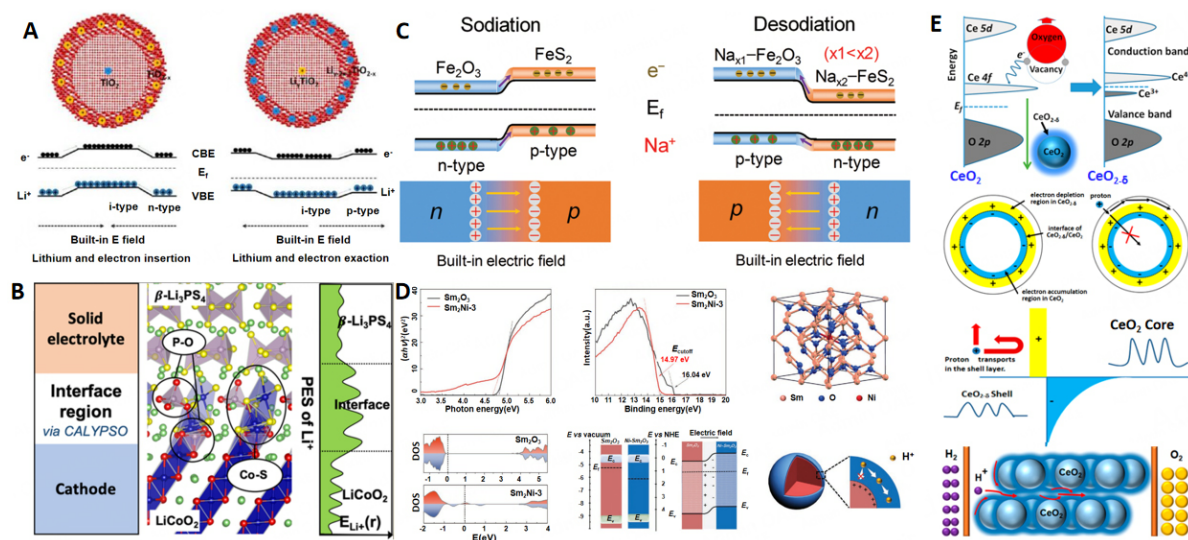


**Figure 4.** Overview of BIEF-enhanced ion transmission in LIBs, Na-ion batteries and CFCs. (A) Illustration of facilitation of  $\text{Li}^+$  charge transport under a BIEF during discharge (left) and charge (right). Copyright from Ref. [13]. (B) Li-ion transport mechanism at heterogeneous  $\text{LiCoO}_2$  cathode/ $\beta\text{-Li}_3\text{PS}_4$  solid electrolyte interface in a LIB. Copyright from Ref. [28]. (C) Schematic of BIEF formation and  $\text{Na}^+$  storage mechanism upon discharge (left) and charge (right) of a Na-ion battery of  $\text{Fe}_2\text{O}_3/\text{Na}_{0.67}(\text{Mn}_{0.67}\text{Ni}_{0.23}\text{Mg}_{0.1})\text{O}_2$ . Further comparison of BIEF-induced high-performance CFCs. Copyright from Ref. [30]. (D) Band diagrams and alignment at  $\text{Sm}_2\text{O}_3/\text{SmNi}$  interface determined from UPS and UV-vis spectroscopy and schematic of proton transport process in SmNi. Copyright from Ref. [31]. (E) BIEF-confined proton transport in  $\text{CeO}_2/\text{CeO}_{2-\delta}$  core-shell structure and illustration of a proton conduction shuttle mechanism. Copyright from Ref. [32].

pathway rather than linear hopping. Two  $\text{PO}_4$  tetrahedral shared faces with octahedra to coordinate interstitial sites mean that the cation rarely occupies the site in the [001] direction<sup>[35]</sup>. Moreover,  $\text{LiFePO}_4$  is also regarded as a small polaron material and the mixed valent state was obtained by partial oxidation. The charge carriers might be holes in  $\text{Li}_{1-y}\text{FePO}_4$  and electrons in the case of  $\text{Li}_x\text{FePO}_4$ . By calculating the long-range electrostatic interactions and observing the high-temperature solid solution state of detached  $\text{LiFePO}_4$ , it is found that Li ions and electrons are highly coupled during the transport process. The activation energies of a hole polaron and a lithium vacancy (0.5 eV) were larger than a single Li ion and an electron (0.37 eV). The lithium disorder occurred at 220 °C, which was the same temperature at which rapid electron hopping commenced<sup>[36]</sup>.

For  $\text{SmNiO}_3$ , chemical doping can lead to a metal-to-insulator transition under isothermal conditions. As Figure 5B shows, in the operating range (300–500 °C), the metallic conductivity of SNO was detrimental to the electrolyte<sup>[37]</sup>. Because of the single electron occupancy on the fourfold degenerate manifold on  $\text{Ni}^{3+}$ , the carriers can move freely without overcoming the on-site Coulombic repulsion. When electrons migrate to the H-SNO parts, the  $e^-$  reduced nickel to  $\text{Ni}^{2+}$  while being suppressed by the Hubbard intra-orbital electron-electron Coulombic interaction ( $U$ ). The filling-controlled Mott transitions of H-SNO mean that it can be used as an electrolyte in CFCs due to the wide electronic band gap. The concentration of protons in SNO was not limited by that of oxygen vacancies, in contrast to typical proton conductors (e.g., yttrium-doped  $\text{BaCeO}_3$  or  $\text{BaZrO}_3$ ). With H and Li doping in  $\text{SmNiO}_3$ , density functional theory calculations verified that H or Li migrated along the [001] direction with a migration barrier of ~0.3 eV for hydrogen and ~0.4 eV for lithium<sup>[38]</sup>, as shown in Figure 5C. In lithiated  $\text{SmNiO}_3$  (Li-SNO), mobile Li ions are located at the interstitial sites of the perovskite, which migrate from the bottom Ni layer to the next Ni layer, resulting in lattice expansion that enhances  $\text{Li}^+$  conduction with a low activation energy. For hydrogenated  $\text{SmNiO}_3$  (H-SNO), high proton conductivity was achieved by converting metallic conducting SNO to the

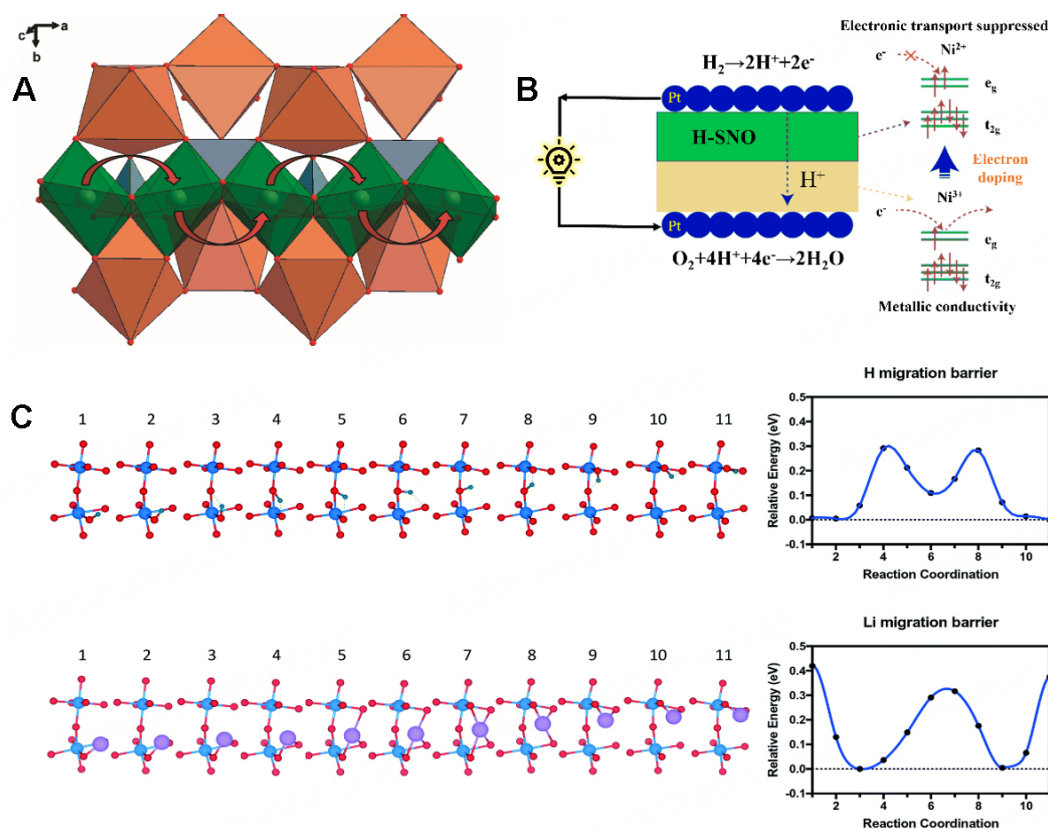


**Figure 5.** (A) Li-ion transport along the b-axis in LiFePO<sub>4</sub>, where the curved trajectories are shown as red arrows, the iron octahedra are orange, the phosphate tetrahedra are blue and lithium ions are green. Copyright from Ref.<sup>[34]</sup>. (B) Schematic of SNO electrolyte working principle in a CFC (left) and the electronic structure of the Ni 3d orbitals of SNO (right). Copyright from Ref.<sup>[37]</sup>. (C) Hydrogen and lithium dopants for migration pathway (left) along [001] direction in SmNiO<sub>3</sub> and its activation energy (right). Copyright from Ref.<sup>[38]</sup>.

electronically insulating phase<sup>[37]</sup>. The  $P_{\max}$  of a fuel cell with Pt electrodes obtained 225 mW/cm<sup>2</sup> with an OCV of 1.03 V at 500 °C. The results of these investigations indicate that the charge transmission pathway has a strong correlation between LIBs and CFCs.

## APPLICATION OF TYPICAL LIB MATERIALS IN CFCS

### LIB materials for single-layer fuel cells

The use of LIB materials in single-layer fuel cells (SLFCs) is an important research area. The first SLFC was reported in 2011 by Zhu *et al.*<sup>[39]</sup>. It was fabricated from one homogeneous layer composed by semiconductors and ionic conductors, as shown in Figure 6A. SLFCs can provide electrochemical performance comparable to that of complex three-layer fuel cells and their simple material preparation and fabrication procedure provide technical advantages. The physical junction always has a crucial effect in overcoming the internal short circuit issue in SLFCs<sup>[40]</sup>. The continuous evolution of LIB materials has resulted in better electronic and Li-ion conductivity while improving the specific capacity, energy density and structural stability. These excellent characteristics provide a reliable basis for the selection of fuel cell materials. In addition to the LiNiZn oxide (LNZ)-(Samarium-doped ceria) SDC composites discussed above, LiNiCuZnFeO<sub>x</sub>-NSDC single components also exhibit impressive cell performance (e.g., 700 mW/cm<sup>2</sup> at 550 °C)<sup>[41]</sup>. The combination of Gadolinium-doped ceria-KAlZn oxide (GDC-KAZ) and LNCZ created an excellent ion transport membrane for single-component fuel cells (SCFCs), which obtained an excellent electrochemical performance of 628 mW/cm<sup>2</sup> at 580 °C, as well as a high ionic

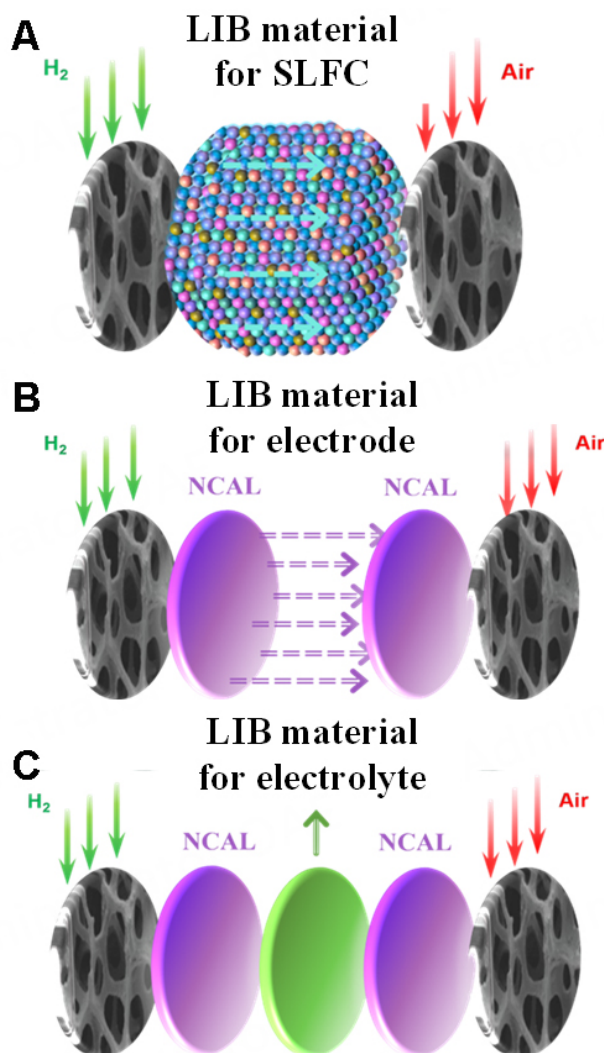


**Figure 6.** LIB materials for (A) SLFCs and as (B) electrodes and (C) electrolytes for CFCs. SLFCs: Single-layer fuel cells; CFCs: ceramic fuel cells.

conductivity of 0.08 S/cm at 600 °C<sup>[42]</sup>. Similarly, a MZSDC-LNCS ( $\text{Mg}_{0.4}\text{Zn}_{0.6}\text{O}/\text{Ce}_{0.8}\text{Sm}_{0.2}\text{O}_{2-\delta}\text{-Li}_{0.3}\text{Ni}_{0.6}\text{Cu}_{0.07}\text{Sr}_{0.03}\text{O}_{2-\delta}$ ) SLFC illustrated a high electrochemical power output of 600 mW/cm<sup>2</sup> at 630 °C<sup>[43]</sup>. A SLFC with a  $\text{Li}_{0.4}\text{Mg}_{0.3}\text{Zn}_{0.3}\text{O}/\text{Ce}_{0.8}\text{Sm}_{0.2}\text{O}_{2-\delta}$  (LMZSDC) composite demonstrated robust durability for over 120 h at 600 °C. AC impedance revealed that LMZSDC had a high ionic conductivity (0.1 S/cm at 600 °C), which contributed to its successful application to SLFCs<sup>[44]</sup>.

Layer-structured  $\text{LiNi}_{0.1}\text{Fe}_{0.90}\text{O}_{2-\delta}$  (LNF) has a good proton conductivity of 0.01-0.1 S/cm at 500-600 °C with competitive electrocatalytic activities. A LNF-composited SDC SLFC showed a power output of 760 mW/cm<sup>2</sup> at 550 °C, where excellent performance was achieved by a simple device structure<sup>[45]</sup>. Hu *et al.* attempted the application of LiNiO-based materials modified with different transition metal elements in SLFCs.  $\text{Li}_{0.3}\text{Ni}_{0.6}\text{Cu}_{0.07}\text{Sr}_{0.03}\text{O}_{2-\delta}$  (LNCuS),  $\text{Li}_{0.3}\text{Ni}_{0.6}\text{Mn}_{0.07}\text{Sr}_{0.03}\text{O}_{2-\delta}$  (LNMnS) and  $\text{Li}_{0.3}\text{Ni}_{0.6}\text{Co}_{0.07}\text{Sr}_{0.03}\text{O}_{2-\delta}$  (LNCoS) were mixed with the ionic conductor SDC, respectively<sup>[46]</sup>. The electrical conductivity of these single-component membranes calculated by electrochemical impedance spectroscopy followed the sequence of 6SDC-4LNMnS > 6SDC-4LNCoS > 6SDC-4LNCuS. The single cell based on the optimized 6SDC-4LNMnS

membrane showed the highest power density of 422 mW/cm<sup>2</sup> at 550 °C<sup>[46]</sup>. In summary, the as-used LIB materials showed three-in-one functions (anode, cathode and electrolyte) in the single-layer devices. The excellent electrical properties of LIB materials represent a new development direction for next-generation fuel cells, which eliminate the traditional three-layer structure with higher electrochemical performance in the low-temperature range.

### LIB materials for CFC electrodes

With the excellent performance of LIB materials, their ion-conducting properties and catalytic effects are expected to play an important role in high-performance CFCs. Indeed, multifunctional lithium materials are being constantly developed for fuel cell devices. Ganesan *et al.* found that LiNiO<sub>2</sub> had high catalytic activity for the ORR at 650 °C for molten carbonate fuel cells<sup>[47]</sup>. Fan *et al.* found that LiNiO<sub>2</sub>-based materials modified by copper, iron and cobalt oxides obtained better electrocatalytic activities and faster charge transfer and gas diffusion rates<sup>[41]</sup>. Additional transition metal elements could be further introduced into LiNiO<sub>2</sub> (separately or simultaneously) based on the advanced NANOCOFC (nanocomposites for advanced fuel cell technology) concept. The as-designed cathode candidates, e.g., lithiated NiCuZnO<sub>x</sub> (LNCZO), showed high compatibility with ceria-carbonate composite electrolyte for low-temperature applications<sup>[41]</sup>. Jing *et al.* prepared LNCZO by a slurry method, which was used as the cathode and anode simultaneously<sup>[18]</sup>. In this report, a samarium-doped NSDC was used as an electrolyte with LNCZ-NSDC symmetrical electrodes. The device achieved a maximum power density of 1000 mW/cm<sup>2</sup> at 470 °C<sup>[18]</sup>. In another work, a novel hierarchically porous LNCZO was designed as symmetrical electrodes matched to the SDC-LiNaCO<sub>3</sub> (LNSDC) electrolyte in CFC, achieving a maximum power density of 132 mW/cm<sup>2</sup> at 550 °C. It was demonstrated that the LNCZO exhibited excellent cathode performance<sup>[19]</sup>. A new triple (H<sup>+</sup>, O<sup>2-</sup> and e<sup>-</sup>)-conducting cathode with layer-structured LiNi<sub>0.8</sub>Co<sub>0.2</sub>O<sub>2</sub> (LNCoO) also showed good ORR activity. The low activation energy (0.88 eV) and evident water uptake capability made the catalytic activity higher than for most cathode materials<sup>[17]</sup>.

NCAL is currently the most widely used symmetric electrode and is compatible with most electrolyte materials in low-temperature CFCs, as shown in [Figure 6B](#). The layered oxide NCAL possesses a crystal structure similar to LNCoO but with improved ORR activity due to the incorporation of Al<sup>3+</sup><sup>[48]</sup>. Yuan *et al.* prepared a uniform NCAL layer on nickel foam by introducing a new coating spraying technology, namely, low-pressure plasma spraying, which was used as an electrode catalytic coating in low-temperature fuel cells<sup>[49]</sup>. Chen *et al.* further revealed that the NCAL electrode had good activity for both the ORR and HOR<sup>[50]</sup>. Furthermore, layered oxide Li(Ni<sub>1/3</sub>Co<sub>1/3</sub>Mn<sub>1/3</sub>)O<sub>2</sub> (LNCM) has been developed as an electrode for symmetric CFCs, which provided lower area-specific resistance than that of a NCAL electrode. LNCM is also a suitable electrode that is compatible with both SDC and BZY, with a power density of 641 mW/cm<sup>2</sup> obtained at 525 °C in a SDC-based symmetric CFC<sup>[51]</sup>. Furthermore, a layer-structured LiCoO<sub>2</sub>-LiFeO<sub>2</sub> heterostructure-based composite was employed as a cathode in a CFC and could be combined with SDC as a composite electrolyte, showing 162 mW/cm<sup>2</sup> at 550 °C. The application of dual-phase-layered lithium-ion composites presents a new direction for the development of high-performance CFCs<sup>[52]</sup>.

### LIB materials for CFC electrolytes

With the successful application of LIB materials as electrodes for low-temperature CFCs, matching electrolytes are also constantly being discovered. The structure of such a CFC is shown in [Figure 6C](#). LIB materials as electrolytes bring surprising electrical properties to CFCs. A chemically stable LiAlO<sub>2</sub>-LiNaCO<sub>3</sub> composite electrolyte was developed to replace doped ceria materials. As Raza *et al.* reported, pure LiAlO<sub>2</sub> (LAO) is an oxygen ionic insulator and the detected current output in the composite electrolyte-based device was mainly from the proton contribution<sup>[53]</sup>. Zhang *et al.* introduced NCAL into a Ce<sub>0.8</sub>Sm<sub>0.2</sub>O<sub>2.8</sub>-Na<sub>2</sub>CO<sub>3</sub> electrolyte to eliminate the polarization between different interfaces<sup>[54]</sup>. The device

reached a high-power density of 1072 mW/cm<sup>2</sup> at 550 °C based on symmetrical NCAL electrodes. Such research demonstrates the extraordinary electrocatalytic and ion-transport ability of NCAL, which can act as both an electrode and electrolyte<sup>[54]</sup>. Furthermore, Lan *et al.* reported a new ionic conducting material, namely, an  $\alpha$ -LiFeO<sub>2</sub>/ $\gamma$ -LiAlO<sub>2</sub> composite, as an electrolyte for CFCs<sup>[55]</sup>. The composite exhibited O<sup>2-</sup> and H<sup>+</sup> co-ionic conduction, reaching 0.50 S/cm at 650 °C under H<sub>2</sub>/air fuel cell conditions<sup>[55]</sup>. Zhu *et al.* added different contents of polyvinylidene fluoride (PVDF) to a LaCePr oxide and NCAL composite electrolyte<sup>[56]</sup>. PVDF was used to improve the triple-phase boundary (TPB) to obtain good electrical performance. The cell achieved a power density of 982 mW/cm<sup>2</sup> at 520 °C<sup>[56]</sup>. A Li-doped ZnO (LZO)/SDC electrolyte showed superionic conductivity (> 0.1 S/cm over 300 °C) without electron leakage and excellent electrolytic performance (400-630 mW/cm<sup>2</sup>) was recorded between 480 and 550 °C<sup>[57]</sup>. Tu *et al.* further revealed that a LZO/SDC composite had a hybrid H<sup>+</sup> and O<sup>2-</sup> conducting capability with predominantly H<sup>+</sup> conduction<sup>[58]</sup>. The proton/Li<sup>+</sup> conductor electrolyte was composed of two-dimensional LiAl<sub>0.5</sub>Co<sub>0.5</sub>O<sub>2</sub> (LACO) nanosheets and amorphous LAO layers. The cell delivered an extremely high P<sub>max</sub> of 1120 mW/cm<sup>2</sup> at 550 °C. The as-designed LAO-coating on LACO can modify the space-charge regions and improve the chemical stability and ionic conductivity of LACO<sup>[59]</sup>. Representative novel CFC configurations and their excellent properties are summarized in Table 1.

## WORKING MECHANISM OF LIB MATERIALS IN CFCs

### Ion transmission mechanism of LIB materials in CFCs

With the application of LIB materials to fuel cells, validating the conduction mechanism of the ionic species under CFC working conditions has become an attractive research frontier. Thus, a review on this topic would provide informative guidance for the rational design and selection of functional materials. Based on the crosslinking between Li<sup>+</sup> and H<sup>+</sup> migration introduced above, most LIB materials used as electrolytes in fuel cells have a layered structure. From the report of Lan *et al.*, protons can be inserted into the Li-deficient Li<sub>x</sub>Al<sub>0.5</sub>Co<sub>0.5</sub>O<sub>2</sub> layer to form Li<sub>x</sub>H<sub>y</sub>Al<sub>0.5</sub>Co<sub>0.5</sub>O<sub>2</sub> at a high temperature, as shown in Figure 7A<sup>[62]</sup>. The proton conductivity of 0.1 S/cm obtained at 500 °C is higher than that of conventional proton-conducting polycrystalline oxides in the same temperature range. The proton intercalation conduction mechanism is different from the oxygen vacancy conduction mechanism in conventional perovskites and doped ceria materials. Aluminum replaced some cobalt sites in LiCoO<sub>2</sub>, which generated a stable sublattice matrix with strongly suppressed electronic conduction. The intrinsic layered structure was well retained and could provide sufficient channels for proton migration. However, the loss of lithium at high temperatures is still a challenging issue. More chemically stable elements (e.g., sodium, potassium and so on) should be considered as alternatives to lithium to achieve more stable proton conductor electrolytes for CFCs<sup>[62]</sup>.

When the electrolyte is composed of a single-phase material, the ion transport usually relies on its crystal structure and the number of intrinsic defects. In recent years, two-phase composites have also been developed as efficient ion conductors, albeit with different conduction mechanisms. As a good example, an  $\alpha$ -LiFeO<sub>2</sub>/ $\gamma$ -LiAlO<sub>2</sub> composite was reported as a novel electrolyte for CFCs. The conductivity of this composite was reasonably high (0.24-0.50 S/cm) at 600-650 °C and orders of magnitude higher than single-phase LiFeO<sub>2</sub> or LiAlO<sub>2</sub>. Moreover, it was found that Li<sup>+</sup>, O<sup>2-</sup> and H<sup>+</sup> ions, as well as electrons, contributed simultaneously to the total conductivity. During the operation of the fuel cell device, both O<sup>2-</sup> and H<sup>+</sup> conduction was clearly detected and the potential difference as a kinetic driving force increased the mobility of O<sup>2-</sup> (or H<sup>+</sup>) ions in LiFeO<sub>2</sub> grains or along the grain boundaries. The possible pathways of ions include the oxygen vacancies in reduced LiFeO<sub>2</sub> and the defects at the LiFeO<sub>2</sub>/LiAlO<sub>2</sub> interface. The combination of semiconducting LiFeO<sub>2</sub> and insulating LAO generated a superionic conductor that provides a new direction for the design of novel ionic conducting materials for CFCs<sup>[55]</sup>. Similarly, Paydar *et al.* reported that proton- and Li<sup>+</sup>-conducting LACO nanosheets coated by a compatible amorphous LAO electrolyte illustrated excellent performance (P<sub>max</sub> of 1120 mW/cm<sup>2</sup> at 550 °C) and improved chemical stability<sup>[59]</sup>. The coated

**Table 1. List of excellent electrical properties of LIB materials in CFCs**

Electrode (anode/cathode)	Electrolyte	Performance tem.	Ref.	
Ag	LiMnO-LiZnO-SDC	210 mW cm <sup>-2</sup> at 550 °C	[60]	
	SDC-LiNiMnSr	422 mW cm <sup>-2</sup> at 550 °C	[46]	
	MgZnO-SDC-LiNiCuSrO	600 mW cm <sup>-2</sup> at 630 °C	[43]	
	GDC-KZnAl-LiNiCuZnO <sub>x</sub>	628 mW cm <sup>-2</sup> at 580 °C	[42]	
	LiNiCuZnO-SDC-(Li/Na) <sub>2</sub> CO <sub>3</sub>	260 mW cm <sup>-2</sup> at 550 °C	[61]	
	Li <sub>x</sub> AlCoO <sub>2</sub>	382 mW cm <sup>-2</sup> at 650 °C	[62]	
Ni foam	SDC-LaSrTiO-NCAL	222 mW cm <sup>-2</sup> at 550 °C	[63]	
Ag/Ni foam	LiNiZnO-SDC	600 mW cm <sup>-2</sup> at 550 °C	[39]	
Ag/Ni foam	LiNiFe oxide-SDC	760 mW cm <sup>-2</sup> at 550 °C	[45]	
Ni-NCAL	NCAL-ZnO-SnO <sub>2</sub>	1267 mW cm <sup>-2</sup> at 530 °C	[64]	
	NCAL-SDC	735 mW cm <sup>-2</sup> at 520 °C	[65]	
	LiNiO-SDC	688 mW cm <sup>-2</sup> at 530 °C	[66]	
	SDC	900 mW cm <sup>-2</sup> at 650 °C	[67]	
	CuFe oxide-LiZnO-SDC	637 mW cm <sup>-2</sup> at 550 °C	[68]	
	LiMgCoO-SDC	700 mW cm <sup>-2</sup> at 600 °C	[69]	
	SDC-Na <sub>2</sub> CO <sub>3</sub> -NCAL	1072 mW cm <sup>-2</sup> at 550 °C	[54]	
	α-Fe <sub>2</sub> O <sub>3</sub> -NCAL	554 mW cm <sup>-2</sup> at 600 °C	[70]	
	LiZnO-SDC	713 mW cm <sup>-2</sup> at 550 °C	[58]	
	LiAlO-LiAlCoO	1120 mW cm <sup>-2</sup> at 550 °C	[59]	
	LiZnO	443 mW cm <sup>-2</sup> at 550 °C	[71]	
	SDC-SrTiO <sub>3</sub>	892 mW cm <sup>-2</sup> at 550 °C	[72]	
	Ni-doped Sm <sub>2</sub> O <sub>3</sub>	1438 mW cm <sup>-2</sup> at 550 °C	[31]	
	Ni-L <sub>x</sub> NCA	SDC	761 mW cm <sup>-2</sup> at 550 °C	[25]
	Lithiated NiCuZnO <sub>x</sub>	SDC-(Li/Na) <sub>2</sub> CO <sub>3</sub>	680 mW cm <sup>-2</sup> at 600 °C	[41]
Ni-LiNiCoMnO	SDC	815 mW cm <sup>-2</sup> at 550 °C	[51]	
LiNiCuZnO	SDC-LiZnO	630 mW cm <sup>-2</sup> at 550 °C	[57]	
Ni-NCAL /LiCoO <sub>2</sub> -LiFeO <sub>2</sub>	SDC-LiCoO <sub>2</sub> -LiFeO <sub>2</sub>	714 mW cm <sup>-2</sup> at 550 °C	[52]	
NiO-CuO composition /Ag	LiAlO <sub>2</sub> -LiNaCO <sub>3</sub>	388 mW cm <sup>-2</sup> at 600 °C	[53]	
Ni-LiNiCoO-SDC- Na <sub>2</sub> CO <sub>3</sub> /NCAL	SDC-Na <sub>2</sub> CO <sub>3</sub> -LiNiCoO	1000 mW cm <sup>-2</sup> at 550 °C	[10]	

LIB: Lithium-ion battery; CFCs: ceramic fuel cells.

core-shell structure and the interface achieved better chemical compatibility for the LAO-LACO composite electrolyte with the NCAL electrode. The special structure made Li<sup>+</sup> more mobile in LAO than in LACO. The imbalanced charge distribution induced Li<sup>+</sup> diffusion from the interface of LAO to the surface of LACO, as shown in Figure 7B. A local electric field was produced by this chemical potential gradient, speeding up H<sup>+</sup> insertion into LAO simultaneously. In addition, Li<sup>+</sup> diffusion on the particle surface region can make a positively charged surface on the LAO-LACO particles, which resist H<sup>+</sup> from further ingressing into LACO, resulting in a proton interfacial conduction mechanism. The local electric field accelerated proton transport through the interface of LAO/LACO<sup>[59]</sup>. These studies suggest the strong correlation of transport paths between Li ions and protons, and moreover, they are helpful for exploring the conduction mechanisms of ions in fuel cells.

### BIEF on LIB materials used in CFCs

The type of composite electrolyte is related to the composite of LIB materials with ionic conductors/semiconductors. For instance, a LiNi<sub>0.8</sub>Co<sub>0.15</sub>Al<sub>0.05</sub>O<sub>2</sub>/Sm<sub>0.2</sub>Ce<sub>0.8</sub>O<sub>2-δ</sub> composite electrolyte was

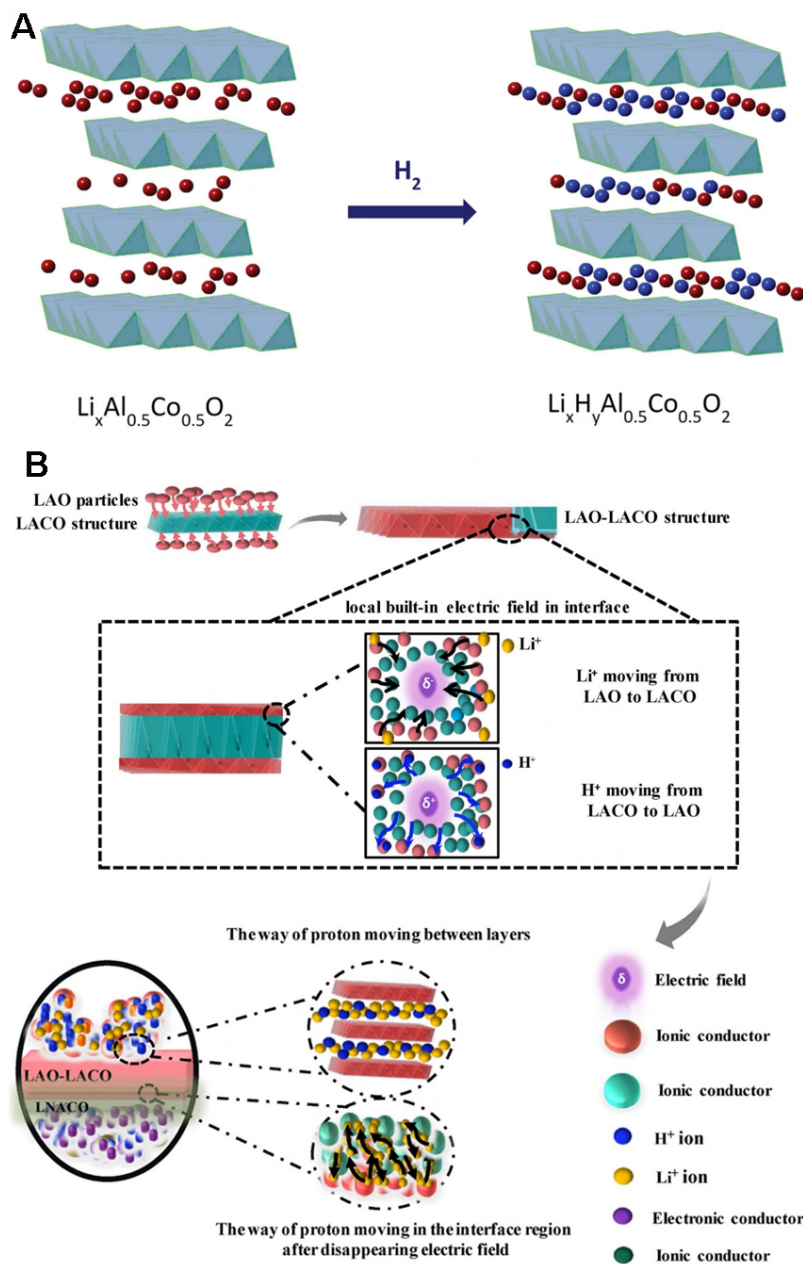


**Figure 7.** Proton conducting transformation of LIB material for the electrolyte of CFCs. (A) Insertion in  $\text{Li}_x\text{Al}_{0.5}\text{Co}_{0.5}\text{O}_2$  in  $\text{H}_2$ . Copyright from Ref. [64]. (B) Transmission in interfacial region between LAO-LACO membrane. Copyright from Ref. [62].

designed using well-tuned energy band structures, thereby providing a promising methodology. A high ionic conductivity (0.12 S/cm at 520 °C) was obtained by 0.5LNCA-1.5SDC in its optimal weight ratio. The heterostructure and reconstruction of energy bands at the two-phase interface play crucial roles in enhancing the ionic conduction and improving the electronic performance of the device<sup>[65]</sup>. In a subsequent study, Liu *et al.* revealed that the ionic conductivity in the composite was higher than the electronic conductivity by orders of magnitude, which exhibited an obvious blocking effect on electrons by the well-tuned heterojunction<sup>[73]</sup>. LNCA-SDC was also identified as a hybrid oxygen ion/proton conducting material<sup>[73]</sup>. In addition, Li-doped ZnO as the electrolyte achieved a remarkable  $P_{\text{max}}$  of 443 mW/cm<sup>2</sup> along

with an OCV of 1.07 V at 550 °C<sup>[71]</sup>. Furthermore, a novel p-n-n heterostructure composite based on p-type NCAL, n-type ZnO and n-type SnO<sub>2</sub> gained the homogenous elemental distribution and heterointerfaces, as well as a greatly increased oxygen vacancy concentration, as shown in [Figure 8A](#). The optimized composition of 2NCAL-1(ZnO-SnO<sub>2</sub>) showed a high ionic conductivity of 0.389 S/cm at 530 °C<sup>[64]</sup>.

Generally, the junction effect can be formed by the contact between p- and n-type semiconductors. The redistribution of charges at the interface can generate a space-charge region, with a BIEF pointed from n- to p-type. By the energy band alignment effect and BIEF, the electronic blocking and ionic acceleration processes are illustrated in [Figure 8B](#). A BIEF can also be formed when utilizing LIB materials as the semiconductor.

Although LIB materials have been widely used as symmetric electrodes in CFCs, the working mechanisms vary under different conditions. For NCAL used as an anode, the lattice structure decomposed in a reducing atmosphere but no significant phase change can be observed as a cathode in fuel cells. These phenomena have raised wide concerns because of the non-negligible effects on the stable operation of fuel cells. As reported by Zhu *et al.*, the structure of Ni-foam/LiNi<sub>0.85</sub>Co<sub>0.15</sub>O<sub>2-δ</sub> (LCN)-NSDC/Ag was designed as a novel Schottky junction fuel cell, as shown in [Figure 8B](#)<sup>[10]</sup>. Based on the principle of a Schottky junction [[Figure 8B](#), left], a potential was built up at the interface between the metal and semiconductor. The metallization of the Ni-containing oxide to Ni helped to catalyze H<sub>2</sub> oxidation on the anode, which formed a remarkable Schottky junction effect with the p-type LCN [[Figure 8B](#), right]. The Schottky junction-induced BIEF played a key role in preventing electrons from passing through the device and accelerating the H<sup>+</sup> transport. Even though silver can function as a cathode, NCAL delivered much better electrochemical performance after replacing the silver cathode<sup>[10]</sup>.

#### ORR and HOR of LIB materials in CFCs

With the application of LIB materials in CFCs, these materials can play the role of electrodes at low temperatures. In CFCs, the ORR at the cathode and the HOR at the anode are key factors affecting the properties of the device. Highly efficient redox reactions in LIB material-based electrodes directly reduce the operating temperature of CFCs and thus these electrodes are suitable for more electrolytes. Therefore, the discussion of the working mechanism of LIB materials as electrodes is of great significance. The enhancement of the catalytic activity of electrodes is an important research topic for conventional CFCs, and this principle should also be considered when utilizing LIB materials as novel CFC electrodes.

The excellent electrochemical performance of NCAL has been observed in many advanced CFC devices due to its high catalytic performance, strong compatibility with the electrolyte and long-term stability. For instance, when NCAL was used as the anode to replace the Pt anode, the  $P_{\max}$  of the device was 32 times higher than that of the Pt anode-coated cell and the ionic conductivity of the electrolyte achieved a 4.4-fold enhancement. Actually, the Li<sup>+</sup> in NCAL has critical effects on the oxidation state and catalytic function. When the NCAL anode was subjected to H<sub>2</sub> reduction, the as-formed chemical potential gradient can drive the diffusion of Li<sup>+</sup> into the electrolyte. For example, LiOH and Li<sub>2</sub>CO<sub>3</sub> produced from NCAL covered the interface of GDC grains, which can form abundant channels for rapid ion transport<sup>[74]</sup>. The bulk conduction mechanism of the GDC electrolyte was changed to an efficient ionic interface conduction mechanism due to the formation of a composite material of LiOH/Li<sub>2</sub>CO<sub>3</sub> in GDC. Li ions accumulated in the multi-phase interface due to their diffusion, resulting in the formation of a SCL. By the principle of electric neutrality, high oxygen vacancy concentrations can be produced to compensate for the loss of the positive charge. The continuous interface network with high oxygen vacancy concentrations provided rapid ionic conduction channels for increasing the ionic conductivity in the GDC electrolyte.

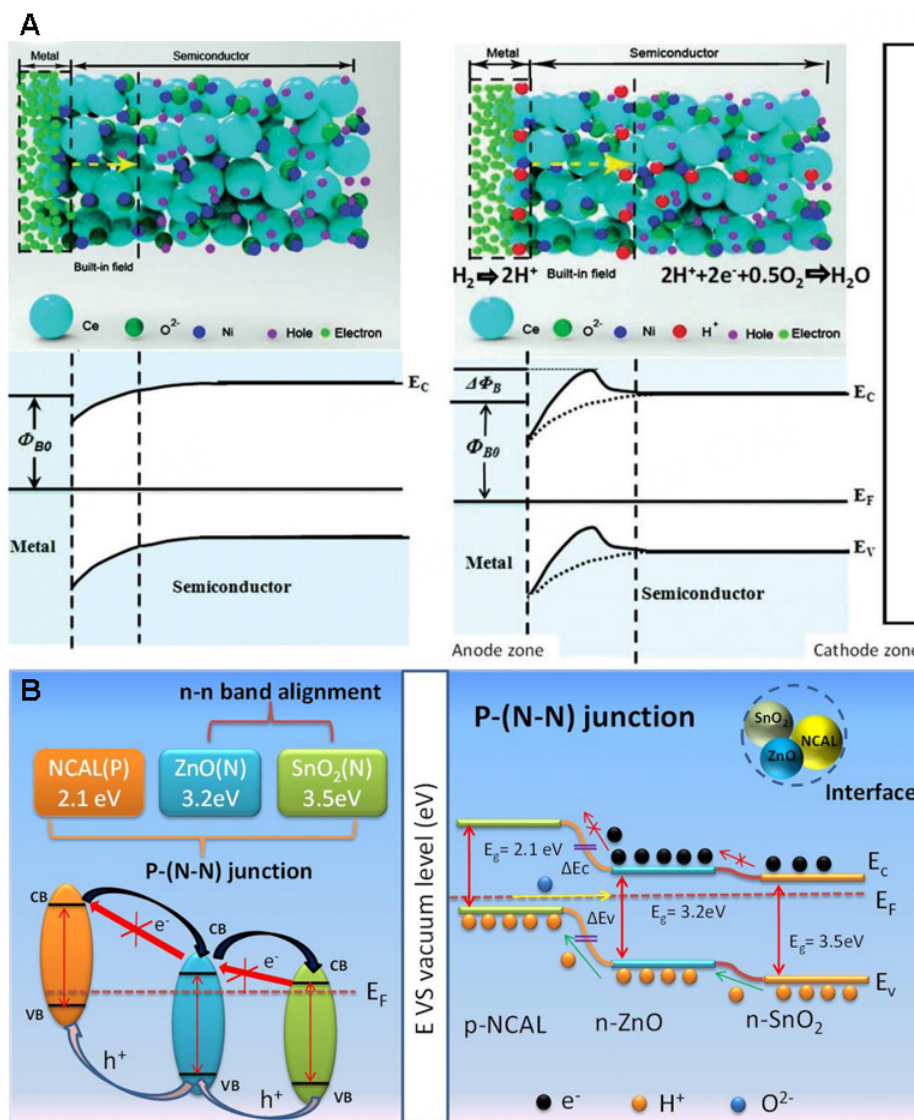


**Figure 8.** Working mechanism of lithium anode in CFCs. (A) Schottky junction of general metal/semiconductor (left) and  $H_2$ -reduced lithium anode/semiconductor (right). Copyright from Ref.<sup>[10]</sup>. (B) Energy band alignment effect for acceleration processes of p-n-heterostructure NCAL-ZnO-SnO<sub>2</sub> electrolyte. Copyright from Ref.<sup>[59]</sup>.

To investigate the effect of lithium by-products on the device, according to the work of Liu *et al.*,  $Li_xNi_{0.8}Co_{0.15}Al_{0.05}O_{2.5}$  ( $L_x$ NCA,  $x = 1.0, 1.2$  or  $1.4$ ) with different lithium contents was designed and prepared as symmetrical electrodes in CFCs<sup>[20]</sup>. The by-products of the NCAL anode under a reducing atmosphere included  $Li_2CO_3$ ,  $LiOH$  and so on. The excessive Li-ion content showed a greater impact on the cathode performance than on the anode<sup>[20]</sup>. This is because  $Li_2CO_3$  and a cation-disordered “NiO-like” shell were formed due to the exposure of NCAL to air, leading to a lower activation energy for the ORR and a higher oxygen ion conductivity<sup>[50]</sup>. Compared with state-of-the-art CFC cathode materials (e.g., LSCF), NCAL displayed a higher ORR activity<sup>[75]</sup> because lithium-ion migration driven by the chemical potential formed a SCL, which enhanced the number of oxygen vacancies at the interface between the cathode and electrolyte. This mechanism facilitated oxygen-ion conduction and reduced the polarization resistance of NCAL<sup>[76]</sup>. Based on the reports of NCAL symmetrical electrodes and their catalytic function, the migration of  $Li^+$  has been confirmed during the fuel cell working process. There might be a certain connection between  $Li^+$  and

other carriers and the migration mode of  $\text{Li}^+$  may have significant effects on the  $\text{H}^+/\text{O}^{2-}/e^-$  triple-phase carriers. Therefore, the migration mechanism of  $\text{Li}^+$  is also of interest in fuel cells.

As revealed by Xia *et al.*, NCAL was considered as a typical lithiated transition metal oxide with triple ( $\text{H}^+/\text{O}^{2-}/e^-$ )-conducting properties and ORR activity<sup>[70]</sup>. The TPB of the electrode regions can be significantly extended under cell operating conditions; thus, the electrode polarizations were decreased accordingly. In addition, the high mobility of  $\text{Li}^+$  in NCAL also dynamically promoted the  $\text{O}^{2-}/\text{H}^+$  transmission<sup>[70]</sup>. Usually, the ORR on the cathode is categorized into four types of H-CFCs, which involve (a) pure electronic conductors (e.g., Pt); (b) mixed ionic and electronic conductors, including  $\text{Ba}_{0.5}\text{Sr}_{0.5}\text{Co}_{0.8}\text{Fe}_{0.2}\text{O}_{3-\delta}$  and  $\text{La}_{0.6}\text{Sr}_{0.4}\text{Co}_{0.2}\text{Fe}_{0.8}\text{O}_{3-\delta}$  (LSCF); (c) mixed protonic and electronic conductors; and (d) triple-conducting oxides that possess three charge carriers, i.e., oxygen ions ( $\text{O}^{2-}$ ), protons ( $\text{H}^+$ ) and electrons ( $e^-$ ) simultaneously in one single-phase material. Triple-conducting cathodes seem to be the most promising class for obtaining high cell performance. As Figure 9 shows, the protons originate from the unique layered structure and the intrinsic high oxygen transport kinetics result in a fast reaction rate of  $\text{H}_2\text{O}$ . The heavy doping of transition metals/alkaline earth metals (Ni, Mn, Cu, Fe, Co and so on) can satisfy sufficient electronic conduction while increasing the electrode catalytic activity. The conductivity and electrode activities of lithiated doped alkali metals can be improved further. For the  $\text{LiNi}_{0.8}\text{CoO}_2$  cathode, the  $e^-/h^+$  conductivity and oxygen vacancies were improved by high  $\text{Ni}^{3+}$  content. Moreover, the protons were driven by lithium intercalation into the layered structure of lithiated oxide and transported by the interspace between two adjacent NiO layers<sup>[17]</sup>.

#### **A liquid-phase approach to improve interfacial ion transport efficiency**

The liquid-like filling method is widely used in many electrochemical devices, which allows the liquid target substance to fill into the medium uniformly and later solidify. The liquid target substance can connect different components of the device tightly and reduce the interfacial resistance to transport ions efficiently. Wei *et al.* designed a capillary action mechanism to enhance the electrolyte density [Figure 10], stating that a liquid phase from the electrode could flow into the narrow space of the electrolyte without the assistance of external forces<sup>[77]</sup>. Based on this principle, a cell with a NCAL/SDC/NiO structure (where 0.5-1.0 wt.% LiOH was added into the NiO anode) was constructed. LiOH was in the liquid state at the cell operating temperature (550 °C), which filled up the pores and gaps in the electrolyte formed by dry pressing. The electrolyte thus became gas-tight and had the ability to separate the fuel and the oxidant. This mechanism provides a good direction to understand the transport process of Li ions in the NCAL anode<sup>[77]</sup>. In fact, a similar approach is used to improve the ionic conductivity in LIBs. The novel electrolyte filling technology could produce supercapacitors and energy density with a photoinitiator coating on the surface of porous carbon nanotubes. The flowing gel polymer electrolytes penetrated into the pores inside the electrode due to gravity. This method provided oxygen diffusion channels<sup>[78]</sup>. Furthermore, solidification is a similar method to convert a liquid into a solid in the solid battery. The liquid precursor with high mobility can fill the voids at the electrode/electrolyte interface and infiltrate the porous cathode. After solidification, the solid components can contact continuously for fluent charge transport and the solid-state batteries can be maximally maintained. This novel method can help to solve the crucial interfacial issues that are related to the rigid and heterogeneous solid-solid contacts between the electrolytes and electrodes<sup>[79]</sup>. As a general strategy, the developed liquid-phase approach showed large-scale industrial prospects for high-efficiency energy applications. The liquid method can promote the reaction sufficiently in solutions and produce homogenous precursors<sup>[80]</sup>. The liquid-phase approach is always used to achieve better electrode/electrolyte interfacial contact, thus improving the performance of fuel cells and batteries. This method is also a fine example of the crosslinking between CFCs and LIBs in terms of performance improvement processes.

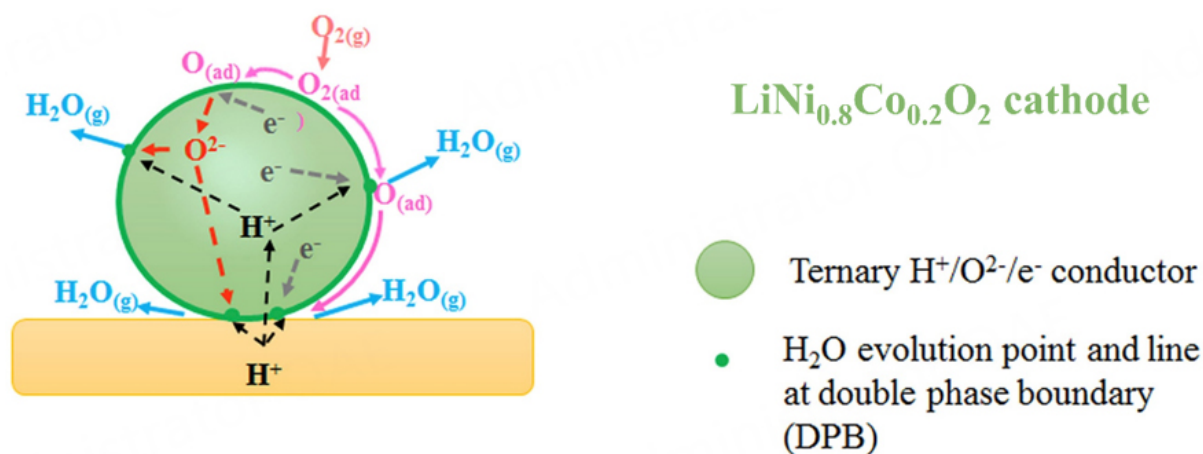


**Figure 9.** Schematic illustration of oxygen reduction and water generation pathways of triple-conducting (H<sup>+</sup>/O<sup>2-</sup>/e<sup>-</sup>) LiNi<sub>0.8</sub>Co<sub>0.2</sub>O<sub>2</sub> cathode for CFCs. Copyright from Ref.<sup>[77]</sup>. CFCs: Ceramic fuel cells.

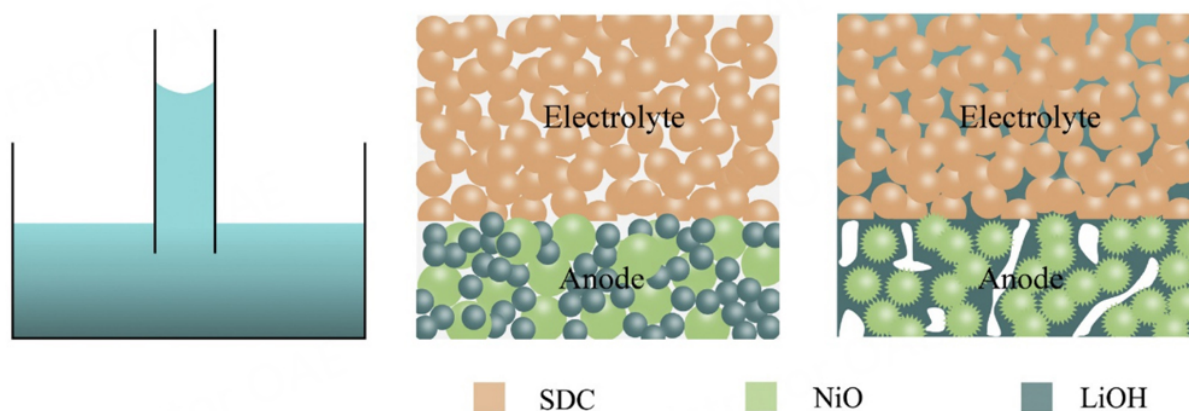


**Figure 10.** The capillary action mechanism of lithium material electrode in CFCs. Copyright from Ref.<sup>[77]</sup>. CFCs: Ceramic fuel cells.

## TYPICAL LIB MATERIALS AND THEIR POTENTIAL APPLICATIONS

As powerful energy storage systems, LIBs can be classified as Li-sulfur batteries, Li-air batteries, organic electrode batteries, solid-state batteries or Li-CO<sub>2</sub> batteries<sup>[81]</sup>. Although LIB techniques have been widely studied, the safety issues induced by liquid-based electrolytes have still not been well addressed. LIBs composed of organic solution electrolytes are prone to leakage and combustion, leading to a series of environmental problems. The development of all-solid-state batteries could be an alternative strategy to avoid these drawbacks, in addition to improved mechanical strength, chemical stability and conductivity (10<sup>-4</sup> to 10<sup>-3</sup> S/cm)<sup>[82]</sup>. The LIB materials transforming into proton conductors mean that their electrochemical properties (e.g., lithium-ion conductivity) have attracted more attention. LIB materials play different roles in all-solid-state batteries, including the cathode, anode and electrolyte. Typical LIB materials are introduced by their roles, which provide a reference for the application of CFCs.

### Typical LIB electrolyte materials

The solid-state electrolyte is a critical component to block electron leakage while transporting lithium ions, which is similar to the electrolytes in CFCs. Li<sub>7</sub>La<sub>3</sub>Zr<sub>2</sub>O<sub>12</sub> (LLZO) is one of the most widely investigated solid electrolytes with a garnet-type structure. The ionic conductivities of the cubic and tetragonal phases of LLZO are 10<sup>-4</sup> and 10<sup>-6</sup> S/cm, respectively<sup>[83]</sup>. However, LLZO cannot retain a stable crystal structure in air,

which is mainly due to the reaction of LLZO with  $\text{CO}_2$  in air to produce a  $\text{Li}_2\text{CO}_3$  passivation layer. The formation of passivation layers reduces ionic conductivity and increases interfacial resistance. Furthermore, NASICONs (sodium super ion conductors), such as  $\text{LiZr}_2(\text{PO}_4)_3$ ,  $\text{LiGe}_2(\text{PO}_4)_3$  and  $\text{Li}_{1.5}\text{Al}_{0.5}\text{Ti}_{1.5}\text{PO}_4$ , have an analogous crystalline structure with the space group of R-3C. For  $\text{Li}_{1.5}\text{Al}_{0.5}\text{Ti}_{1.5}\text{PO}_4$ , the  $\text{PO}_4$  tetrahedra alternate and corner share with  $[\text{TiO}_6]$  octahedra, where the Li species occupy interstitial sites<sup>[84]</sup>. In addition, Li-S batteries have attracted significant interest due to their high theoretical energy density and gravimetric capacity<sup>[14]</sup>. Furthermore, widely-used sulfide ( $\text{Li}_2\text{S-SiS}_2$  and  $\text{Li}_2\text{S-P}_2\text{S}_5$ ) and perovskite ( $\text{LiLaTiO}_3$ ) materials have shown higher conductivity ( $10^{-2}$  S/cm), lower grain boundary resistance and excellent flexibility<sup>[33]</sup>. In 1979, a Li salt complexed with a solid polymer electrolyte (SPE) was used in the first all-solid-state film battery. The SPE usually consists of a polymer matrix and lithium salts<sup>[85]</sup>. The all-solid-state polymer electrolyte and quasi-solid-state polymer electrolyte are attractive candidates for Li-S cells with excellent flexibility and mechanical stability<sup>[86]</sup>. With the continuous development of this field, polymer electrolyte materials with different kinds of transporting ions (e.g.,  $\text{H}^+$ ,  $\text{Li}^+$ ,  $\text{Na}^+$ ,  $\text{K}^+$  and  $\text{Ag}^+$ ) have been explored extensively in academia and industry. SPEs have also shown significant potential for a variety of solid-state power sources, such as secondary batteries, fuel cells and supercapacitors<sup>[87]</sup>. The special structures of LIB electrolytes with different ion transport mechanisms make it possible for their practical use in CFCs. Good Li-ion conductivity of the materials is an ideal property for CFCs.

### Typical LIB electrode materials

In LIBs, the basis of the power supply comes from the Li-ion shuttle between the electrode materials; thus, the electrode performance can be evaluated by the Li-ion insertion ability. The electrode material can be divided into three types: intercalation; conversion; alloying<sup>[88]</sup>.

Intercalation-type electrode materials mainly provide intercalation and deintercalation sites for  $\text{Li}^+$  in the lattice, which is usually dominated by layered structure materials, with the most representative materials including  $\text{LiNiO}_2$  and  $\text{LiCoO}_2$ <sup>[89]</sup>. The layered structure facilitates the diffusion and insertion of Li ions, accelerating the battery charging speed.  $\text{LiCoO}_2$  as the most famous electrode material was invented by Goodenough and coworkers in the 1980s, which led to a significant increase in the battery voltage (4 V) compared with previous ones (< 2.5 V)<sup>[23]</sup>. Subsequently,  $\text{LiMn}_2\text{O}_4$ , as another famous three-dimensional spinel-structured electrode material, achieved a reduced cost. The crystal structure of  $\text{LiMn}_2\text{O}_4$  is similar to  $\text{LiCoO}_2$  and possesses a cubic close-packed oxygen lattice with edge-sharing octahedra, as well as excellent  $\text{Li}^+$  and electronic conductivities<sup>[90]</sup>. Generally, the transition metal elements in layered materials can induce a change in the valence states (e.g.,  $\text{Ni}^{3+}$  to  $\text{Ni}^{2+}$  in  $\text{LiNiO}_2$ ) during the processes of  $\text{Li}^+$  intercalation and deintercalation, leading to disordered cation sites in the crystal. Studies have shown that the disorder can disrupt the transport path of lithium ions and with the effect of the electrostatic repulsion between transition metal elements, the Li mobility can be significantly reduced. Simultaneously, the Li slab space can also be reduced due to the disorder effect, resulting in a high activation barrier to Li-ion diffusion<sup>[91]</sup>. To address these challenges, the doping of polymetallic elements was developed to stabilize the crystal structure, and thus the disadvantage of single doping can be avoided with additional advantages, e.g., enhanced electrical properties. Recently,  $\text{LiNi}_x\text{Co}_y\text{Mn}_{1-x-y}\text{O}_2$  (NCM)<sup>[92]</sup> and  $\text{LiNi}_x\text{Co}_y\text{Al}_{1-x-y}\text{O}_2$  (NCA) have attracted significant attention as new-generation LIB electrodes because of their higher specific capacity and energy density<sup>[93]</sup>. For example, the optimized composition of  $\text{LiNi}_{0.8}\text{Co}_{0.15}\text{Al}_{0.05}\text{O}_2$  has been used in Tesla's electric vehicles with improved cost-effectiveness. The addition of low-cost transition metals (e.g.,  $\text{Ni}^{2+}$  and  $\text{Al}^{3+}$ ) not only increased its specific capacity, but also solved the safety issue related to the  $\text{O}_2$  evolution from the material. Additionally, NMC with the same crystal structure has been commercialized for the electronics to electric vehicles applications due to its high volumetric and gravimetric capacity, high nominal voltage and low self-discharge<sup>[94]</sup>.

There are numerous transition metal oxides, nitrogen compounds, sulfides and phosphides that can be classified as the conversion-type anodes. In conversion-type materials, the structural change induced by chemical interactions is usually irreversible due to the conversion reaction between  $\text{Li}^+$  and the corresponding element without the provision of intercalation sites, but offers a large area for rapid diffusion of  $\text{Li}^+$  at the surface of the anode and electrolyte<sup>[95]</sup>. Simultaneously, the charge transport motion mechanics can be enhanced by the exposed active surface. Several newly-developed anodes containing large polyanions  $(\text{XO}_4)^{y-}$  ( $\text{X} = \text{S}, \text{P}, \text{Si}, \text{As}, \text{Mo}$  or  $\text{W}$ ) can promote the ORR and stabilize the lattice structure. However, polyanion-containing anodes still have shortcomings, such as poor electronic conductivity compared with intercalation-type ones<sup>[96]</sup>. Furthermore,  $\text{Li}^+$  diffuses in one dimension, resulting in lower lithium-ion conductivity in  $\text{LiFePO}_4$ . Recently, surface decoration with carbon materials has been identified as an effective strategy to improve the conductivity of  $\text{LiFePO}_4$ .  $\text{LiFePO}_4$  has promoted the development of other anionic materials in lithium-/sodium-ion batteries, such as  $\text{LiMnPO}_4$ ,  $\text{Na}_2\text{FePO}_4\text{F}$ ,  $\text{Na}_3\text{V}_2(\text{PO}_4)_2\text{F}_3$  and  $\text{Li}_2\text{MSiO}_4$  ( $\text{M} = \text{Mn}, \text{Fe}, \text{Co}$  or  $\text{Ni}$ )<sup>[97]</sup>. Compared with the less stable high-valent redox couples ( $\text{Co}^{3+/4+}$  and  $\text{Ni}^{3+/4+}$ ), the low-valent redox couples ( $\text{Fe}^{2+/3+}$ ) are more stable. The stronger bonding from large polyanions can inhibit oxygen release from the lattice and enhance the thermal stability.

The third type of LIB electrode material is alloys, where lithium always reacts with the IVA, VA groups of alloys, including Si, Ge, Sn, Pb, P, As, Sb and Bi. In addition, Sn-Si hybrid materials have shown both high specific capacity and good cycle stability for potential applications in electric vehicles<sup>[98]</sup>. Ni- and Co-based oxynitrides can be readily prepared as stable and dendrite-free lithium anodes, which keep the battery safe and maintain a high specific energy. A nitride of  $\text{Li}_3\text{N}$  can be in-situ formed by  $\text{NiCoON}$ , which can enhance the electronic and ionic conductivity for the kinetic induction of the homogeneous deposition of  $\text{Li}$ <sup>[99]</sup>. In fact, multi-element doping is beneficial to increasing the ion conductivity and enhances the catalysis in CFCs. The solid electrolyte interphase (SEI) plays an important role in the long-term durability of the battery, by which the electrolyte component can be readily protected from decomposition by forming solid products at the interface (i.e., a passivation layer). However, the complex reduction pathways of multiple components in the electrolyte can form random SEIs and unstable SEIs can bring continuous cracking and reconstruction<sup>[100]</sup>. Some reports showed that the formation of the SEI layer is highly related to the inorganic components ( $\text{MF}$  and  $\text{M}_2\text{CO}_3$ ,  $\text{M} = \text{Li}, \text{Na}$  or  $\text{K}$ ) and the  $\text{MF}$  has a critical function in improving the interfacial stability. Therefore, constructing stable SEI films on the electrode surface to achieve a stabilized microstructure deserves more attention<sup>[101]</sup>. In addition, organic electrode materials are becoming more popular because of their advantages of low cost, safety, environmental friendliness, design diversity and low-temperature applications<sup>[102]</sup>. Modulating lithiophilicity at the electrode/electrolyte interface can improve the interfacial  $\text{Li}$  mobility, where in-situ formed polymers in contact with the anode are highly flexible<sup>[103]</sup>. In addition, the next generation of LIB electrodes has been developed, as shown in [Figure 11](#)<sup>[104]</sup>, and the more competitive LIB materials with excellent properties are listed in [Table 2](#).

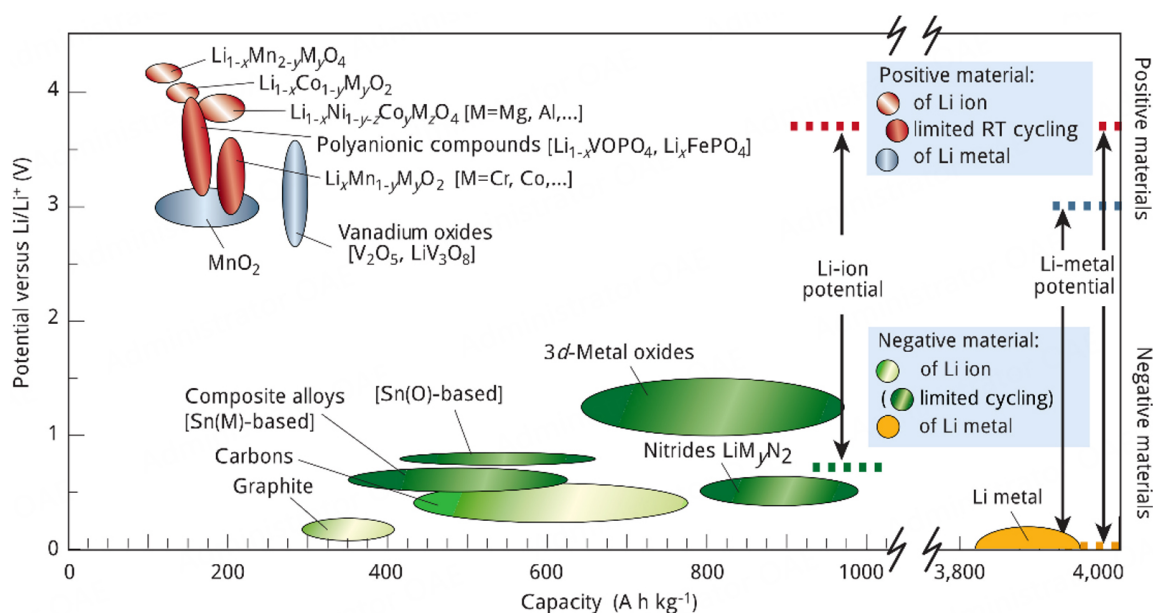
It is noteworthy that the special structure of a LIB material as an electrode forms the transport pathway of  $\text{Li}^+$  and the improved interface between the electrode and electrolyte can promote the diffusion of  $\text{Li}^+$ . These mechanisms are particularly relevant and can be crosslinked to CFCs. Based on the good electrochemical properties of LIB materials, some of them have been successfully used in fuel cells and played better roles at lower operating temperatures.

## SUMMARY AND PERSPECTIVE

The works discussed in this review have opened a new way and methodology for the rational design of new ionic conductors and functional materials with tuned energy band structures. The application of LIB materials in fuel cells is a valuable and promising crosslink research field. Based on the state-of-the-art

**Table 2. Commonly used lithium electrode/electrolyte materials (the conductivity for the electrolytes is ionic conductivity and for the electrodes is electronic conductivity)**

Application	Structure	Material	Properties of lithium material	Ref.
Electrolyte	Garnet	$\text{Li}_7\text{La}_3\text{Zr}_2\text{O}_{12}$	Ionic conductivity of $10^{-4}$ S/cm	[83]
		$\text{Li}_5\text{La}_3\text{M}_2\text{O}_{12}$ (M = Nb, Ta)	Ionic conductivity of $10^{-6}$ S/cm	[105]
		$\text{Li}_{6.5}\text{La}_3\text{Zr}_{1.5}\text{Ta}_{0.5}\text{O}_{12}$	Ionic conductivity of $1.27 \times 10^{-3}$ S/cm	[106]
	NASICON	$\text{Li}_{1.5}\text{Al}_{0.5}\text{Ti}_{1.5}\text{PO}_4$	Ionic conductivity of $7 \times 10^{-4}$ S/cm	[84]
	Perovskite	$\text{LiLaTiO}_3$	Ionic conductivity of $10^{-2}$ S/cm	[33]
	LISICON	$\text{Li}_{14}\text{ZnGe}_4\text{O}_{16}$	Ionic conductivity of $10^{-7}$ S/cm	[107]
Electrode	Layered	$\text{LiNiO}_2$	Theoretical specific capacity of 275 mAh/g	[108]
		$\text{LiCoO}_2$	Ionic conductivity of $10^{-3}$ S/cm	[109]
		$\text{LiNi}_{0.8}\text{Co}_{0.15}\text{Al}_{0.05}\text{O}_2$	Initial discharge capacity of 201.2 mAh/g	[110]
		$\text{LiNi}_x\text{Mn}_y\text{Co}_{1-x-y}\text{O}_2$	Specific capacity 122.21 mA h/g	[111]
	Olivine	$\text{LiFePO}_4$	Ionic conductivity of $5 \times 10^{-8}$ S/cm	[112]
		$\text{LiMnPO}_4$	Specific capacity 168 mAh/g	[113]
	Spinel	$\text{LiMn}_2\text{O}_4$	Ionic conductivity of $1.81 \times 10^{-4}$ S/cm	[114]
	Tavorite	$\text{LiFeSO}_4\text{F}$	Ionic conductivity of $1.65 \times 10^{-4}$ S/cm	[15]

**Figure 11.** Voltage versus capacity for electrode materials presently used in LIBs. Copyright from Ref. [104]. LIBs: Lithium-ion batteries.

research and development, the unique semiconductor properties of the electrodes, e.g., DOS and band, as well as BIEF, relevant crystal structure, electrical properties and electron/ion coupling properties, are the keys and common scientific principles to support their applications in CFCs. Among them, layer-structured LIB materials (e.g., NCAL and  $\text{LiCoO}_2$ ) play the important roles of electrode and electrolyte in CFCs and facilitate proton transport and HOR/ORR functions, leading to enhanced power outputs. It is expected that layered materials, such as  $\text{LiTiO}_2$ ,  $\text{LiNiO}_2$  or lithium garnet-type oxide LLZO, with optimized electronic and ionic conductivities can be well applied to next-generation fuel cells. From the perspective of materials design, the doping strategy with transition metal elements cannot only enhance the catalytic function of the raw material, but also reduce the production cost and stabilize the crystal structure to obtain more durable CFC devices. In parallel, the development of heterostructure composites<sup>[115]</sup> for surface and interface

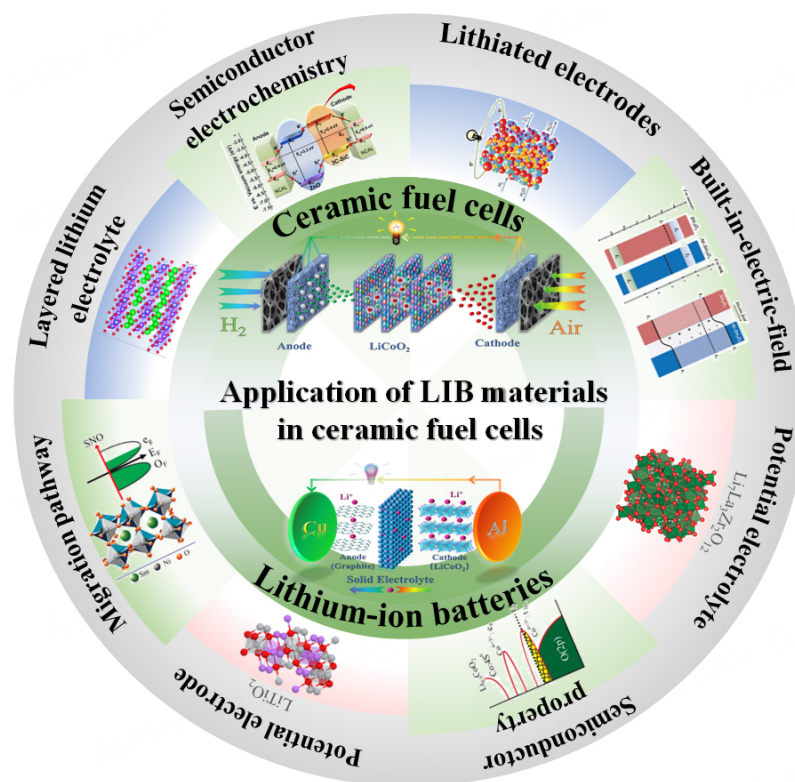


Figure 12. A summary of the advanced applications of LIB materials in CFCs.

functionalities can further develop multiple functions of these materials for practical applications. In addition, spinel-, garnet- and perovskite-type crystal structures also played a significant role in promoting ion transport in the electrolytes of CFCs. Some polyanionic sulfates and fluorides show a high affinity for protons due to the enrichment of anionic groups, thereby promoting the proton transport process.

In LIBs, the development of new structured materials to facilitate the intercalation and deintercalation of lithium ions has been identified as an important research direction. In fuel cells, the migration of lithium ions also has a significant impact on cell performance, which deserves further in-depth studies. The layered crystal structure promoting the migration of lithium ions can also generate highly efficient migration paths for protons<sup>[62]</sup>. The reported high-performance CFCs using LIB materials as electrolytes and electrodes possess a similar physical structure to advanced all-solid-state lithium batteries. The participation of lithium and the resultant products have shown a promotion effect on the ion transport and thus the energy conversion efficiency of fuel cells<sup>[116]</sup>. The coupling effect between lithium ions and electrons was regarded as the key to improving the energy storage in the battery. In contrast, in semiconductor membrane-based fuel cells employing LIB materials, the coupling mechanism cannot only increase the ionic conductivity, but also improve the energy conversion efficiency. Figure 12 summarizes the strong correlation of working mechanisms between LIBs and CFCs, illustrating the potential of lithium materials for common applications in both devices. More LIB materials are expected to have significant potential for further research and development in advanced CFCs.

## DECLARATIONS

### Authors' contributions

Conceived and designed the manuscript: Wang B

Prepared tables: Yang J, Wang R

Prepared figures: Zhou X, Yang J, Wang R

Discussed and commented on the manuscript: Zhang W, Yun S, Wang B

Wrote the paper: Zhou X, Zhang W

All authors participated in the data analysis and results discussions, and commented on the manuscript.

### Availability of data and materials

Not applicable.

### Financial support and sponsorship

National Natural Science Foundation of China (Grant No. 51872080), Key Program for International S&T Cooperation Projects of Shaanxi Province (2019KWZ-03), Key Program for Nature Science Foundation of Shaanxi Province (2019JZ-20), and Key Science and Technology Innovation Team of Shaanxi Province (2022TD-34).

### Conflicts of interest

All authors declared that there are no conflicts of interest.

### Ethical approval and consent to participate

Not applicable.

### Consent for publication

Not applicable.

### Copyright

©The Author(s) 2022.

## REFERENCES

1. Cao X, Zhang L, Huang K, Zhang B, Wu J, Huang Y. Strained carbon steel as a highly efficient catalyst for seawater electrolysis. *Energy Mater* 2022;2:200010. DOI
2. Zhu B, Mi Y, Xia C, et al. A nanoscale perspective on solid oxide and semiconductor membrane fuel cells: materials and technology. *Energy Mater* 2022;1:100002. DOI
3. Stambouli A, Traversa E. Solid oxide fuel cells (SOFCs): a review of an environmentally clean and efficient source of energy. *Renew Sustain Energy Rev* 2002;6:433-55. DOI
4. Chang H, Wu Y, Han X, Yi T. Recent developments in advanced anode materials for lithium-ion batteries. *Energy Mater* 2022;1:100003. DOI
5. Maleki H, Howard JN. Role of the cathode and anode in heat generation of Li-ion cells as a function of state of charge. *J Power Sources* 2004;137:117-27. DOI
6. Curi M, Ferraz H, Furtado J, Secchi A. Dispersant effects on YSZ electrolyte characteristics for solid oxide fuel cells. *Ceram Int* 2015;41:6141-8. DOI
7. Raza R, Zhu B, Rafique A, Naqvi MR, Lund P. Functional ceria-based nanocomposites for advanced low-temperature (300-600 °C) solid oxide fuel cell: a comprehensive review. *Mater Today Energy* 2020;15:100373. DOI
8. Sebastian L, Jayashree RS, Gopalakrishnan J. Probing the mobility of lithium in LISICON: Li<sup>+</sup>/H<sup>+</sup> exchange studies in Li<sub>2</sub>ZnGeO<sub>4</sub> and Li<sub>2+2x</sub>Zn<sub>1-x</sub>GeO<sub>4</sub>. *J Mater Chem* 2003;13:1400-5. DOI
9. Wei T, Zhang LA, Chen Y, Yang P, Liu M. Promising proton conductor for intermediate-temperature fuel cells: Li<sub>13.9</sub>Sr<sub>0.1</sub>Zn(GeO<sub>4</sub>)<sub>4</sub>. *Chem Mater* 2017;29:1490-5. DOI
10. Zhu B, Lund PD, Raza R, et al. Schottky junction effect on high performance fuel cells based on nanocomposite materials. *Adv Energy Mater* 2015;5:1401895. DOI
11. Enslin D, Cherkashinin G, Schmid S, Bhuvaneshwari S, Thissen A, Jaegermann W. Nonrigid band behavior of the electronic

- structure of LiCoO<sub>2</sub> thin film during electrochemical Li deintercalation. *Chem Mater* 2014;26:3948-56. DOI
12. Manthiram A, Goodenough JB. Lithium-based polyanion oxide cathodes. *Nat Energy* 2021;6:844-5. DOI
  13. Xia T, Zhang W, Murowchick J, Liu G, Chen X. Built-in electric field-assisted surface-amorphized nanocrystals for high-rate lithium-ion battery. *Nano Lett* 2013;13:5289-96. DOI PubMed
  14. Ruan J, Sun H, Song Y, et al. Constructing 1D/2D interwoven carbonous matrix to enable high-efficiency sulfur immobilization in Li-S battery. *Energy Mater* 2022;1:100018. DOI
  15. Guo Z, Zhang D, Qiu H, et al. Improved cycle stability and rate capability of graphene oxide wrapped tavorite LiFeSO<sub>4</sub>F as cathode material for lithium-ion batteries. *ACS Appl Mater Interfaces* 2015;7:13972-9. DOI
  16. Wang L, Xie R, Chen B, et al. In-situ visualization of the space-charge-layer effect on interfacial lithium-ion transport in all-solid-state batteries. *Nat Commun* 2020;11:5889. DOI PubMed PMC
  17. Fan L, Su P. Layer-structured LiNi<sub>0.8</sub>Co<sub>0.2</sub>O<sub>2</sub>: A new triple (H<sup>+</sup>/O<sub>2</sub><sup>-</sup>/e<sup>-</sup>) conducting cathode for low temperature proton conducting solid oxide fuel cells. *J Power Sources* 2016;306:369-77. DOI
  18. Jing Y, Qin H, Liu Q, Singh M, Zhu B. Synthesis and electrochemical performances of LiNiCuZn oxides as anode and cathode catalyst for low temperature solid oxide fuel cell. *J Nanosci Nanotechnol* 2012;12:5102-5. DOI PubMed
  19. Zhao Y, He Y, Fan L, et al. Synthesis of hierarchically porous LiNiCuZn-oxide and its electrochemical performance for low-temperature fuel cells. *Int J Hydrogen Energy* 2014;39:12317-22. DOI
  20. Liu X, Dong W, Tong Y, et al. Li effects on layer-structured oxide Li<sub>x</sub>Ni<sub>0.8</sub>Co<sub>0.15</sub>Al<sub>0.05</sub>O<sub>2.6</sub>: improving cell performance via on-line reaction. *Electrochim Acta* 2019;295:325-32. DOI
  21. Mushtaq N, Lu Y, Xia C, et al. Design principle and assessing the correlations in Sb-doped Ba<sub>0.5</sub>Sr<sub>0.5</sub>FeO<sub>3-δ</sub> perovskite oxide for enhanced oxygen reduction catalytic performance. *J Catal* 2021;395:168-77. DOI
  22. Zhu B, Fan L, Mushtaq N, et al. Semiconductor electrochemistry for clean energy conversion and storage. *Electrochem Energy Rev* 2021;4:757-92. DOI
  23. Goodenough JB, Park KS. The Li-ion rechargeable battery: a perspective. *J Am Chem Soc* 2013;135:1167-76. DOI PubMed
  24. Becker D, Cherkashinin G, Hausbrand R, Jaegermann W. Adsorption of diethyl carbonate on LiCoO<sub>2</sub> thin films: formation of the electrochemical interface. *J Phys Chem C* 2014;118:962-7. DOI
  25. Wang B, Zhu B, Yun S, et al. Fast ionic conduction in semiconductor CeO<sub>2-δ</sub> electrolyte fuel cells. *NPG Asia Mater* 2019;11. DOI
  26. Xing Y, Hu E, Wang F, et al. Cubic silicon carbide/zinc oxide heterostructure fuel cells. *Appl Phys Lett* 2020;117:162105. DOI
  27. Lu Y, Zhu B, Shi J, Yun S. Advanced low-temperature solid oxide fuel cells based on a built-in electric field. *Energy Mater* 2022;1:100007. DOI
  28. Gao B, Jalem R, Ma Y, Tateyama Y. Li<sup>+</sup> Transport mechanism at the heterogeneous cathode/solid electrolyte interface in an all-solid-state battery via the first-principles structure prediction scheme. *Chem Mater* 2020;32:85-96. DOI
  29. Rauf S, Zhu B, Shah M, et al. Low-temperature solid oxide fuel cells based on Tm-doped SrCeO<sub>2-δ</sub> semiconductor electrolytes. *Mater Today Energy* 2021;20:100661. DOI
  30. Ni J, Sun M, Li L. Highly efficient sodium storage in iron oxide nanotube arrays enabled by built-in electric field. *Adv Mater* 2019;31:e1902603. DOI PubMed
  31. Wang F, Hu E, Wu H, et al. Surface-engineered homostructure for enhancing proton transport. *Small Methods* 2022;6:e2100901. DOI PubMed
  32. Xing Y, Wu Y, Li L, et al. Proton shuttles in CeO<sub>2</sub>/CeO<sub>2-δ</sub> core-shell structure. *ACS Energy Lett* 2019;4:2601-7. DOI
  33. Wang Y, Wu Y, Wang Z, Chen L, Li H, Wu F. Doping strategy and mechanism for oxide and sulfide solid electrolytes with high ionic conductivity. *J Mater Chem A* 2022;10:4517-32. DOI
  34. Ellis BL, Lee KT, Nazar LF. Positive electrode materials for Li-ion and Li-batteries. *Chem Mater* 2010;22:691-714. DOI
  35. Morgan D, Van der Ven A, Ceder G. Li conductivity in Li<sub>x</sub>MPO<sub>4</sub> (M = Mn, Fe, Co, Ni) olivine materials. *Electrochem Solid-State Lett* 2004;7:A30. DOI
  36. Gibot P, Casas-Cabanas M, Laffont L, et al. Room-temperature single-phase Li insertion/extraction in nanoscale Li<sub>x</sub>FePO<sub>4</sub>. *Nat Mater* 2008;7:741-47. DOI
  37. Zhou W, Shao Z. Fuel cells: hydrogen induced insulation. *Nat Energy* 2016;1:16078. DOI
  38. Yoo P, Liao P. Metal-to-insulator transition in SmNiO<sub>3</sub> induced by chemical doping: a first principles study. *Mol Syst Des Eng* 2018;3:264-74. DOI
  39. Zhu B, Raza R, Abbas G, Singh M. An electrolyte-free fuel cell constructed from one homogenous layer with mixed conductivity. *Adv Funct Mater* 2011;21:2465-9. DOI
  40. Shao K, Li F, Zhang G, Zhang Q, Maliutina K, Fan L. Approaching durable single-layer fuel cells: promotion of electroactivity and charge separation via nanoalloy redox exsolution. *ACS Appl Mater Interfaces* 2019;11:27924-33. DOI PubMed
  41. Fan L, Zhang H, Chen M, et al. Electrochemical study of lithiated transition metal oxide composite as symmetrical electrode for low temperature ceramic fuel cells. *Int J Hydrogen Energy* 2013;38:11398-405. DOI
  42. Zhu B, Fan L, Zhao Y, Tan W, Xiong D, Wang H. Functional semiconductor-ionic composite GDC-KZnAl/LiNiCuZnOx for single-component fuel cell. *RSC Adv* 2014;4:9920. DOI
  43. Hu H, Lin Q, Zhu Z, Zhu B, Liu X. Fabrication of electrolyte-free fuel cell with Mg<sub>0.4</sub>Zn<sub>0.6</sub>O/Ce<sub>0.8</sub>Sm<sub>0.2</sub>O<sub>2-δ</sub>-Li<sub>0.3</sub>Ni<sub>0.6</sub>Cu<sub>0.07</sub>Sr<sub>0.03</sub>O<sub>2-δ</sub> layer. *J Power Sources* 2014;248:577-81. DOI
  44. Hu H, Lin Q, Zhu Z, Liu X, Zhu B. Time-dependent performance change of single layer fuel cell with Li<sub>0.4</sub>Mg<sub>0.3</sub>Zn<sub>0.3</sub>O/Ce<sub>0.8</sub>Sm<sub>0.2</sub>O<sub>2-δ</sub>

- composite. *Int J Hydrogen Energy* 2014;39:10718-23. DOI
45. Zhu B, Fan L, Deng H, et al. LiNiFe-based layered structure oxide and composite for advanced single layer fuel cells. *J Power Sources* 2016;316:37-43. DOI
  46. Hu H, Lin Q, Muhammad A, Zhu B. Electrochemical study of lithiated transition metal oxide composite for single layer fuel cell. *J Power Sources* 2015;286:388-93. DOI
  47. Ganesan P, Colon H, Haran B, White R, Popov BN. Study of cobalt-doped lithium-nickel oxides as cathodes for MCFC. *J Power Sources* 2002;111:109-20. DOI
  48. Zhang W, Cai Y, Wang B, et al. The fuel cells studies from ionic electrolyte  $\text{Ce}_{0.8}\text{Sm}_{0.05}\text{Ca}_{0.15}\text{O}_{2-\delta}$  to the mixture layers with semiconductor  $\text{Ni}_{0.8}\text{Co}_{0.15}\text{Al}_{0.05}\text{LiO}_{2-\delta}$ . *Int J Hydrogen Energy* 2016;41:18761-8. DOI
  49. Yuan K, Zhu J, Dong W, et al. Applying low-pressure plasma spray (LPPS) for coatings in low-temperature SOFC. *Int J Hydrogen Energy* 2017;42:22243-9. DOI
  50. Chen G, Sun W, Luo Y, et al. Investigation of layered  $\text{Ni}_{0.8}\text{Co}_{0.15}\text{Al}_{0.05}\text{LiO}_2$  in electrode for low-temperature solid oxide fuel cells. *Int J Hydrogen Energy* 2018;43:417-25. DOI
  51. Wang K, Zheng D, Cai H, et al. Rational design of favourite lithium-ion cathode materials as electrodes for symmetrical solid oxide fuel cells. *Ceram Int* 2021;47:30536-45. DOI
  52. Liu Y, Xia C, Wang B, Tang Y. Layered  $\text{LiCoO}_2\text{-LiFeO}_2$  heterostructure composite for semiconductor-based fuel cells. *Nanomaterials* 2021;11:1224. DOI PubMed PMC
  53. Raza R, Gao Z, Singh T, Singh G, Li S, Zhu B.  $\text{LiAlO}_2\text{-LiNaCO}_3$  composite electrolyte for solid oxide fuel cells. *J Nanosci Nanotechnol* 2011;11:5402-7. DOI PubMed
  54. Zhang W, Cai Y, Wang B, et al. Mixed ionic-electronic conductor membrane based fuel cells by incorporating semiconductor  $\text{Ni}_{0.8}\text{Co}_{0.15}\text{Al}_{0.05}\text{LiO}_{2-\delta}$  into the  $\text{Ce}_{0.8}\text{Sm}_{0.2}\text{O}_{2-\delta}\text{-Na}_2\text{CO}_3$  electrolyte. *Int J Hydrogen Energy* 2016;41:15346-53. DOI
  55. Lan R, Tao S. High ionic conductivity in a  $\text{LiFeO}_2\text{-LiAlO}_2$  composite under  $\text{H}_2$ /air fuel cell conditions. *Chem A Eur J* 2015;21:1350-8. DOI PubMed
  56. Zhu J, Deng H, Zhu B, et al. Polymer-assistant ceramic nanocomposite materials for advanced fuel cell technologies. *Ceram Int* 2017;43:5484-9. DOI
  57. Fan L, Ma Y, Wang X, Singh M, Zhu B. Understanding the electrochemical mechanism of the core-shell ceria-LiZnO nanocomposite in a low temperature solid oxide fuel cell. *J Mater Chem A* 2014;2:5399. DOI
  58. Tu Z, Tian Y, Liu M, et al. Remarkable ionic conductivity in a LZO-SDC composite for low-temperature solid oxide fuel cells. *Nanomaterials* 2021;11:2277. DOI PubMed PMC
  59. Paydar S, Peng J, Huang L, et al. Performance analysis of  $\text{LiAl}_{0.5}\text{Co}_{0.5}\text{O}_2$  nanosheets for intermediate-temperature fuel cells. *Int J Hydrogen Energy* 2021;46:26478-88. DOI
  60. Zhu B, Fan L, He Y, Zhao Y, Wang H. A commercial lithium battery LiMn-oxide for fuel cell applications. *Mater Lett* 2014;126:85-8. DOI
  61. Pan C, Tan W, Lu J, Zhu B. Microstructure and catalytic activity of  $\text{Li}_{0.15}\text{Ni}_{0.25}\text{Cu}_{0.3}\text{Zn}_{0.3}\text{O}_{2-\delta}\text{-Ce}_{0.8}\text{Sm}_{0.2}\text{O}_{1.9}\text{-carbonate}$  nanocomposite materials functioning as single component fuel cell. *Int J Hydrogen Energy* 2014;39:19140-7. DOI
  62. Lan R, Tao S. Novel proton conductors in the layered oxide material  $\text{LiAl}_{0.5}\text{Co}_{0.5}\text{O}_2$ . *Adv Energy Mater* 2014;4:1301683. DOI
  63. Gao J, Xu S, Akbar M, et al. Single layer low-temperature SOFC based on  $\text{Ce}_{0.8}\text{Sm}_{0.2}\text{O}_{2-\delta}\text{-La}_{0.25}\text{Sr}_{0.75}\text{TiO}_{3-\delta}\text{-Ni}_{0.8}\text{Co}_{0.15}\text{Al}_{0.05}\text{LiO}_{2-\delta}$  composite material. *Int J Hydrogen Energy* 2021;46:9775-81. DOI
  64. Lu Y, Akbar M, Li J, Ma L, Wang B, Xia C. A p-n-n heterostructure composite for low-temperature solid oxide fuel cells. *J Alloys Compd* 2022;890:161765. DOI
  65. Tayyab Z, Rauf S, Xia C, et al. Advanced LT-SOFC based on reconstruction of the energy band structure of the  $\text{LiNi}_{0.8}\text{Co}_{0.15}\text{Al}_{0.05}\text{O}_2\text{-Sm}_{0.2}\text{Ce}_{0.8}\text{O}_{2-\delta}$  heterostructure for fast ionic transport. *ACS Appl Energy Mater* 2021;4:8922-32. DOI
  66. Lu Y, Akbar M, Xia C, et al. Catalytic membrane with high ion-electron conduction made of strongly correlated perovskite  $\text{LaNiO}_3$  and  $\text{Ce}_{0.8}\text{Sm}_{0.2}\text{O}_{2-\delta}$  for fuel cells. *J Catal* 2020;386:117-25. DOI
  67. Akbar M, Alvi F, Shakir MI, et al. Effect of sintering temperature on properties of LiNiCuZn-Oxide: a potential anode for solid oxide fuel cell. *Mater Res Express* 2019;6:105505. DOI
  68. Zhang J, Zhang W, Xu R, Wang X, Yang X, Wu Y. Electrochemical properties and catalyst functions of natural CuFe oxide mineral-LZSDC composite electrolyte. *Int J Hydrogen Energy* 2017;42:22185-91. DOI
  69. Ganesh KS, Wang B, Kim J, Zhu B. Ionic conducting properties and fuel cell performance developed by band structures. *J Phys Chem C* 2019;123:8569-77. DOI
  70. Xia C, Afzal M, Wang B, et al. Mixed-conductive membrane composed of natural hematite and  $\text{Ni}_{0.8}\text{Co}_{0.15}\text{Al}_{0.05}\text{LiO}_{2-\delta}$  for electrolyte layer-free fuel cell. *Adv Mater Lett* 2017;8:114-21. DOI
  71. Xia C, Qiao Z, Shen L, et al. Semiconductor electrolyte for low-operating-temperature solid oxide fuel cell: Li-doped ZnO. *Int J Hydrogen Energy* 2018;43:12825-34. DOI
  72. Cai Y, Chen Y, Akbar M, et al. A bulk-heterostructure nanocomposite electrolyte of  $\text{Ce}_{0.8}\text{Sm}_{0.2}\text{O}_2\text{-delta-SrTiO}_3$  for low-temperature solid oxide fuel cells. *Nanomicro Lett* 2021;13:46. DOI PubMed PMC
  73. Liu X, Dong W, Xia C, et al. Study on charge transportation in the layer-structured oxide composite of SOFCs. *Int J Hydrogen Energy* 2018;43:12773-81. DOI
  74. He Y, Chen G, Zhang X, et al. Mechanism for major improvement in SOFC electrolyte conductivity when using lithium compounds

- as anode. *ACS Appl Energy Mater* 2020;3:4134-8. DOI
75. Fan Q, Yan S, Wang H. Nanoscale redox reaction unlocking the next-generation low temperature fuel cell. *Energy Mater* 2022;2:200002. DOI
  76. Yang D, Chen G, Liu H, et al. Electrochemical performance of a  $\text{Ni}_{0.8}\text{Co}_{0.15}\text{Al}_{0.05}\text{LiO}_2$  cathode for a low temperature solid oxide fuel cell. *Int J Hydrogen Energy* 2021;46:10438-47. DOI
  77. Wei L, Dong W, Yuan M, et al. Interface engineering towards low temperature in-situ densification of SOFC. *Int J Hydrogen Energy* 2020;45:10030-8. DOI
  78. Peng X, Wang C, Liu Y, et al. Critical advances in re-engineering the cathode-electrolyte interface in alkali metal-oxygen batteries. *Energy Mater* 2022;1:100011. DOI
  79. Bi Z, Guo X. Solidification for solid-state lithium batteries with high energy density and long cycle life. *Energy Mater* 2022;2:200011. DOI
  80. Su H, Jiang Z, Liu Y, et al. Recent progress of sulfide electrolytes for all-solid-state lithium batteries. *Energy Mater* 2022;2:200005. DOI
  81. Bashir T, Ismail SA, Song Y, et al. A review of the energy storage aspects of chemical elements for lithium-ion based batteries. *Energy Mater* 2022;1:100019. DOI
  82. Xia S, Wu X, Zhang Z, Cui Y, Liu W. Practical challenges and future perspectives of all-solid-state lithium-metal batteries. *Chem* 2019;5:753-85. DOI
  83. Dermenci KB, Çekiç E, Turan S. Al stabilized  $\text{Li}_7\text{La}_3\text{Zr}_2\text{O}_{12}$  solid electrolytes for all-solid state Li-ion batteries. *Int J Hydrogen Energy* 2016;41:9860-7. DOI
  84. Anantharamulu N, Koteswara Rao K, Rambabu G, Vijaya Kumar B, Radha V, Vithal M. A wide-ranging review on Nasicon type materials. *J Mater Sci* 2011;46:2821-37. DOI
  85. Yadav P, Beheshti SH, Kathribail AR, Ivanchenko P, Mierlo JV, Berecibar M. Improved performance of solid polymer electrolyte for lithium-metal batteries via hot press rolling. *Polymers* 2022;14:363. DOI PubMed PMC
  86. Castillo J, Qiao L, Santiago A, et al. Perspective of polymer-based solid-state Li-S batteries. *Energy Mater* 2022;2:200003. DOI
  87. Uitz M, Epp V, Bottke P, Wilkening M. Ion dynamics in solid electrolytes for lithium batteries. *J Electroceram* 2017;38:142-56. DOI
  88. Wang L, Świątowska J, Dai S, et al. Promises and challenges of alloy-type and conversion-type anode materials for sodium-ion batteries. *Mater Today Energy* 2019;11:46-60. DOI
  89. Fleischmann S, Kamboj I, Augustyn V. Nanostructured transition metal oxides for electrochemical energy storage. In Nanda J, Augustyn V, editors, *Transition Metal Oxides for Electrochemical Energy Storage*. 2022. pp. 183-212. DOI
  90. Williams QL, Adepoju AA, Zaab S, Doumbia M, Alqahtani Y, Adebayo V. Application of carbon nanomaterials on the performance of Li-ion batteries. In Misra P, editor, *Spectroscopy and Characterization of Nanomaterials and Novel Materials*. 2022. pp. 361-414. DOI
  91. Chernova NA, Ma M, Xiao J, Whittingham MS, Breger J, Grey CP. Layered  $\text{Li}_x\text{Ni}_y\text{Mn}_z\text{Co}_{1-2y}\text{O}_2$  cathodes for Lithium ion batteries: understanding local structure via magnetic properties. *Chem Mater* 2007;19:4682-93. DOI
  92. Zhang X, Liu G, Zhou K, et al. Enhancing cycle life of nickel-rich  $\text{LiNi}_{0.9}\text{Co}_{0.05}\text{Mn}_{0.05}\text{O}_2$  via a highly fluorinated electrolyte additive - pentafluoropyridine. *Energy Mater* 2021;1:100005. DOI
  93. Yang Z, Zheng C, Wei Z, et al. Multi-dimensional correlation of layered Li-rich Mn-based cathode materials. *Energy Mater* 2022;2:200006. DOI
  94. Du Z, Wood DL, Daniel C, Kalnaus S, Li J. Understanding limiting factors in thick electrode performance as applied to high energy density Li-ion batteries. *J Appl Electrochem* 2017;47:405-15. DOI
  95. Kim H, Krishna T, Zeb K, et al. A comprehensive review of Li-ion battery materials and their recycling techniques. *Electronics* 2020;9:1161. DOI
  96. Hautier G, Jain A, Chen H, Moore C, Ong SP, Ceder G. Novel mixed polyanions lithium-ion battery cathode materials predicted by high-throughput ab initio computations. *J Mater Chem* 2011;21:17147. DOI
  97. Li J, Yao W, Martin S, Vaknin D. Lithium ion conductivity in single crystal  $\text{LiFePO}_4$ . *Solid State Ionics* 2008;179:2016-9. DOI
  98. Shao Y, Jin Z, Li J, Meng Y, Huang X. Evaluation of the electrochemical and expansion performances of the Sn-Si/graphite composite electrode for the industrial use. *Energy Mater* 2022;2:200004. DOI
  99. Wang Y, Xu H, Zhong J, et al. Hierarchical Ni- and Co-based oxynitride nanoarrays with superior lithiophilicity for high-performance lithium metal anodes. *Energy Mater* 2022;1:100012. DOI
  100. Xiao Y, Xu R, Xu L, Ding J, Huang J. Recent advances in anion-derived SEIs for fast-charging and stable lithium batteries. *Energy Mater* 2022;1:100013. DOI
  101. Zhang L, Chen Y. Electrolyte solvation structure as a stabilization mechanism for electrodes. *Energy Mater* 2022;1:100004. DOI
  102. Huang T, Long M, Xiao J, Liu H, Wang G. Recent research on emerging organic electrode materials for energy storage. *Energy Mater* 2022;1:100009. DOI
  103. Li C, Zhang X, Zhu Y, et al. Modulating the lithiophilicity at electrode/electrolyte interface for high-energy Li-metal batteries. *Energy Mater* 2022;1:100017. DOI
  104. Tarascon JM, Armand M. Issues and challenges facing rechargeable lithium batteries. *Nature* 2001;414:359-67. DOI PubMed
  105. Thangadurai V, Kaack H, Weppner WJF. Novel fast lithium ion conduction in garnet-type  $\text{Li}_5\text{La}_3\text{M}_2\text{O}_{12}$  (M:Nb,Ta). *ChemInform*

- 2003;34. DOI
106. Kataoka K, Akimoto J. High ionic conductor member of garnet-type oxide  $\text{Li}_{6.5}\text{La}_3\text{Zr}_{1.5}\text{Ta}_{0.5}\text{O}_{12}$ . *ChemElectroChem* 2018;5:2551-7. DOI
  107. Jasinski G, Jasinski P, Chachulski B, Nowakowski A. Lisicon solid electrolyte electrocatalytic gas sensor. *J Eur Ceram Soc* 2005;25:2969-72. DOI
  108. Ma Y, Teo JH, Kitsche D, et al. Cycling performance and limitations of  $\text{LiNiO}_2$  in solid-state batteries. *ACS Energy Lett* 2021;6:3020-8. DOI
  109. Tukamoto H, West AR. Electronic conductivity of  $\text{LiCoO}_2$  and its enhancement by magnesium doping. *J Electrochem Soc* 1997;144:3164-8. DOI
  110. Xiao P, Lv T, Chen X, Chang C.  $\text{LiNi}_{0.8}\text{Co}_{0.15}\text{Al}_{0.05}\text{O}_2$ : enhanced electrochemical performance from reduced cationic disordering in Li slab. *Sci Rep* 2017;7:1408. DOI
  111. Liu Y, Liu M. Reproduction of Li battery  $\text{LiNi}_x\text{Mn}_y\text{Co}_{1-x-y}\text{O}_2$  positive electrode material from the recycling of waste battery. *Int J Hydrogen Energy* 2017;42:18189-95. DOI
  112. Orikasa Y, Gogyo Y, Yamashige H, et al. Ionic conduction in lithium ion battery composite electrode governs cross-sectional reaction distribution. *Sci Rep* 2016;6:26382. DOI PubMed PMC
  113. Choi D, Wang D, Bae IT, et al.  $\text{LiMnPO}_4$  nanoplate grown via solid-state reaction in molten hydrocarbon for Li-ion battery cathode. *Nano Lett* 2010;10:2799-805. DOI PubMed
  114. Rao B, Padmaraj O, Narsimulu D, Venkateswarlu M, Satyanarayana N. A.C conductivity and dielectric properties of spinel  $\text{LiMn}_2\text{O}_4$  nanorods. *Ceram Int* 2015;41:14070-7. DOI
  115. Shah MY, Lu Y, Mushtaq N, et al. ZnO/MgZnO heterostructure membrane with type II band alignment for ceramic fuel cells. *Energy Mater* 2022;2:200031. DOI
  116. Chen G, Liu H, He Y, et al. Electrochemical mechanisms of an advanced low-temperature fuel cell with a  $\text{SrTiO}_3$  electrolyte. *J Mater Chem A* 2019;7:9638-45. DOI